Bulletin of Engineering Geology and the Environment (2022) 81: 391
https://doi.org/10.1007/s10064-022-02884-9

ORIGINAL PAPER

Effects of layer thickness and temperature on desiccation cracking characteristics of coral clay

Huaqiang Fang[1,2] · Xuanming Ding[1,2] · Chunyong Jiang[1,2] · Yu Peng[3] · Chunyan Wang[1,2]

Received: 12 September 2021 / Accepted: 12 August 2022 / Published online: 30 August 2022

Abstract

Coral clay is one of the products of sorting sediments from the reclamation of coral islands. To reveal the crack characteristics of coral clay(C) with different layer thickness and temperature, a series of physiochemical and desiccation cracking tests are conducted, as well as the contrast tests of Chongqing silt (S), Kaolin (K) and Talcum (T). The results show that coral clay is a kind of low liquid limit clay (CL) composed of fine-grained coral debris and appears pale yellow and soft muddy with high water content. Its particle composition contents of silt, clay and sand are 56%, 42% and 2% respectively. The main mineral composition of coral clay is Aragonite, Calcite and Calcite magnesian, and the content is up to 39.5%, 35.5% and 25%, respectively. Coral clay, Chongqing silt and talcum under different layer thicknesses and temperatures all show a significant crack network. The area of soil clods separated by the cracks increases with the increment of layer thickness; accordingly, the number of the clod is decreased. Compared with coral clay, Chongqing silt and talcum, Kaolin has better cracked resistance. The fractal dimensions of coral clay, Chongqing silt and talcum all increase with the increment of layer thickness. Fractal dimensions of coral clay and Chongqing silt both increase slowly with the increase of temperature. Moreover, there is a good exponential relationship between the fractal dimension and average crack width. The frequency distributions of the crack length and width of coral clay under different layer thicknesses all conform to the form of Log-Normal function curve. Besides, the crack morphology is multi-scale. The current work provides a reference for the possible future applications of this new material.

Keywords Crack characteristics · Coral clay · Layer thickness · Desiccation cracking · Laboratory test

Introduction

Cracks are widespread in nature and our lives, such as cracks on the surface of fine-grained soil and cohesive soil, cracks in building wall paint, pavement cracks, cracks in rockfill dam panels, and bark patterns. Figure 1 shows cracks on the surface of a certain interior wall paint. In general, cracks will occur during drying or cold shrinking. The mechanical morphology of the cracks mostly shows the form of polygonal cracks on the surface, and the study of its formation mechanism is a hot spot in mechanics, materials science and earth science (Bordoloi et al. 2018; Niu et al. 2019; Peron et al. 2009; Sánchez and Al-Taie 2020).

Soil desiccation cracking has been being a hot research topic so far (Abd El-Halim 2017; Bordoloi et al. 2020; Colombi et al. 2021; Obada et al. 2020; Wang et al. 2018a; Wei et al. 2020; Zhang et al. 2015). The drying process can cause the soil to shrink and crack under normal circumstances. The formation of cracks not only destroys the soil structure, but also greatly affects its strength, deformation as well as permeability, which triggers a series of engineering accidents and geological environmental problems (Li and Zhang 2011; Lozada et al. 2015; Senior 1981; Zhang et al. 2020a; Yin et al. 2022). In terms of soil types and soil composition, Baer et al. (2009) evaluated soil crack patterns evolving over time for exposed surfaces with claypan soils. Shin and Santamarina (2011) studied the cracks of fine-grained

✉ Xuanming Ding
dxmhhu@163.com

1 College of Civil Engineering, Chongqing University, Chongqing 400045, China

2 Key Laboratory of New Technology for Construction of Cities in Mountain Area, Ministry of Education, Chongqing 400045, China

3 Department of Civil and Environmental Engineering, The Hong Kong Polytechnic University, Hung Hom, Kowloon, Hong Kong, China

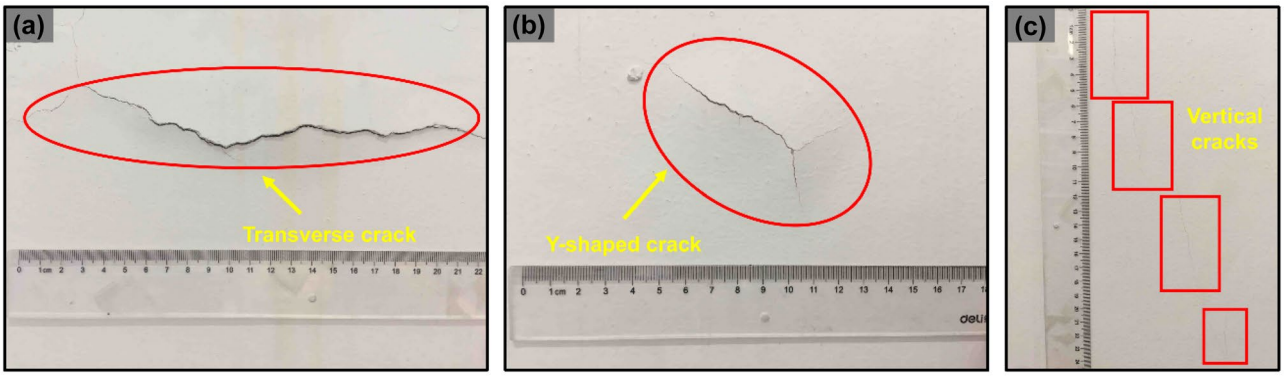

Fig. 1 Typical cracks in wall paint

soils and pointed out that the mechanical model of tensile strength is used to explain the formation of dry cracks in the soil. On the basis of a series of laboratory tests, Costa et al. (2013) conducted desiccation tests on three materials, Merri Creek and Werribee clay, potato starch and milled quartz sand, and discussed some factors governing soil desiccation cracking. Tran et al. (2019a) studied the desiccation cracking of a Cutanic Luvisol on a small scale. Mei et al. (2020) used biochar to relieve sand cracks. An et al. (2020); Cheng et al. (2020); Liu et al. (2020); Tang et al. (2020); Tang et al. (2019); Wang et al. (2018b); Zeng et al. (2019); Zeng et al. (2020); Zhang et al. (2020b) conducted a large number of laboratory experiments on Nanjing Xiashu soil, which mainly involved the influencing factors of cracking (such as layer thickness, interfacial friction, dry and wet cycles), of soil modification (such as biochar, microbial modification), of compacted soil, of crack characterization (such as resistivity method, CT technology). Mohammad et al. (2020) studied the cracking law of bentonite and discussed the influence of initial moisture content and layer thickness on the bentonite drying cracks. Julina and Thyagaraj (2020) used XCT technology to quantitatively study the volume behavior and crack morphology of compacted clay in a certain area of India. Emmanuel and Anggraini (2020) conducted laboratory tests on Malaysian high-plastic marine clay and studied the laws of samples' cracking. Xie et al. (2020) studied the combined effects of the addition of nylon fiber and an enzyme-containing product on crack initiation of Merri-Creek clay. The commonest clay minerals of shale, such as montmorillonite, illite, kaolinite, were experimentally studied by (Shepidchenko et al. 2020) to show the main controlling factors of desiccation cracks and the influence of these factors on crack geometry. At present, the research on cracking involves a wide range of soil types, but there are currently few researches on the phenomenon of coral clay cracking.

In recent years, large-scale land reclamation projects based on coral islands have been carried out in several countries (Chen et al. 2021; Peng et al. 2021, 2019; Pancrazi et al. 2020; Van Impe et al. 2015; Zainal et al. 2012). During the refilling of coral reefs, coral clay interlayers composed of fine-grained coral debris have been formed. Coral clay, as the muddy interlayer of the foundation, has an important influence on the deformation and strength characteristics of the foundation. Figure 2 shows the coral clay in the hydraulic fill foundation shrinks during the process of losing water, then cracks (Qin et al. 2021). Cracks in the foundation can seriously affect the safety of the buildings on the islands and reefs. The slopes of islands and reefs may also cause cracks due to uneven shrinkage of coral clay, which affects its stability. Meanwhile, the generation of cracks will cause permeability damage due to the change of water table. Given the scarcity of construction materials on islands and reefs, the coral clay, local materials on coral islands, can be used as a building material, which has high economic benefits. Currently, coral clay-related construction putty and coatings are being developed. Coral clay, as a building material, cracks during its drying process. Therefore, it is necessary to study the development of shrinkage cracks in coral clay. It is of great significance to study the causes of coral clay cracking, the initiation and propagation of cracks, and the mechanical mechanisms.

Fig. 2 Desiccation cracking phenomenon of coral clay foundation in calcareous sand filling site in Saudi RSGT project (Qin et al. 2021)

Previous studies mainly focused on common clay materials. However, as a high-quality coral clay that can be used for building materials from local materials, its composition is very different from the general clay, and the research on its cracking characteristics is rarely carried out. In this paper, the characteristics of coral clay cracking are investigated through laboratory tests, in order to provide a reference for the possible future applications of this new material. Considering the influence of layer thickness on the final crack morphology, the physical and chemical properties and the morphology of macroscopic cracks of coral clay and other comparison samples were obtained through physical property test, XRF test, XRD diffraction test and desiccation cracking test. Combined with electron microscope test, the morphological characteristics of soil microcracks were discussed. Moreover, the soil desiccation cracking mechanism was discussed. The influence rule of multi-scale crack morphology of coral clay under the influence of layer thickness was finally obtained.

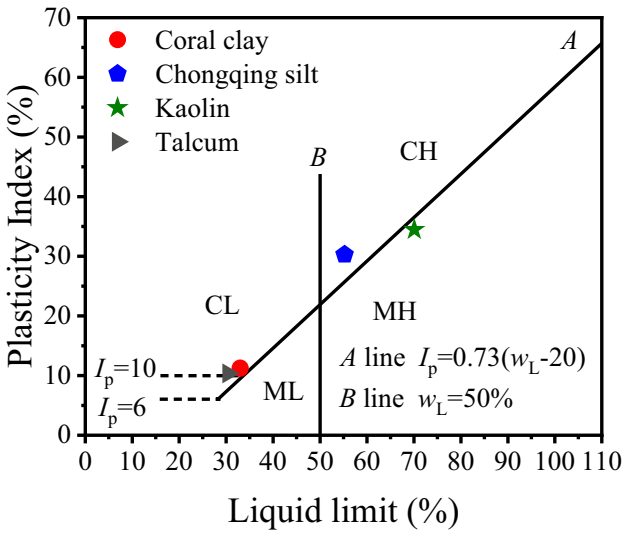

Fig. 4 Plasticity chart

Materials and methods

Soils

Coral clay used in this experiment is taken from a certain area in the South China Sea, which is a calcareous soft mud composed of fine-grained coral debris (Shen et al. 2018). It is necessary to conduct a comparative study with other types of silt. For instance, Chongqing silt (S) from a certain area of Chongqing is selected as a comparative sample. Coral clay (C), from the aspect of being building materials, kaolin (K), talcum (T), being used as building materials, are all selected as comparative samples to study characteristics of desiccation cracking. The depth of coral clay is 0 ~ 0.5 m, as shown in Fig. 3(a1). It is a light yellow calcareous soft mud composed of fine-grained coral debris, mixed with blue-gray silt, and its organic matter content is 0.4%. The color of the dried coral clay is light yellow, as shown in Fig. 3(a2). The color of Chongqing silt is brown-gray, and the depth of soil is 0 ~ 0.5 m, and its organic matter content is 2.19%. Similarly, Chongqing silt after drying is also brown-gray, as shown in Fig. 3(b). Kaolin and talcum, high purity and white color, are purchased from the market, as shown in Fig. 3(c) and (d), respectively. The basic physical properties of the four soils are shown in Table 1.

Figure 4 is a plasticity chart, through which the above four types of fine-grained soils can be classified. Combining Table 1 and Fig. 4, we can conclude that Coral clay, Chongqing silt, kaolin and talcum belong to low liquid limit clay (CL), high liquid limit clay (CH), high liquid limit silt (MH) and low liquid limit clay (CL), respectively. Coral clay particles are mainly composed of silt and clay, with extremely low sand content. The composition of Chongqing silt particles is mainly silt, followed by clay, and contains a small amount of sand; the composition of kaolin does not contain sand, but is mainly silt and clay. The composition of talcum is mainly silt and contains a small amount of clay and sand.

Figure 5 shows the cumulative curve of particle size distribution of different soils, which can reflect the size of soil particles, the uniformity of particle size distribution, and the degree of continuity of distribution. From Fig. 5, the characteristic particle diameters, uneven coefficients and curvature coefficients of different soils can be obtained, as shown in Table 2.

The soil unevenness coefficient (C_u) is used to characterize the degree of uniformity of the soil, which can reflect the size difference between coarse particles and fine particles.

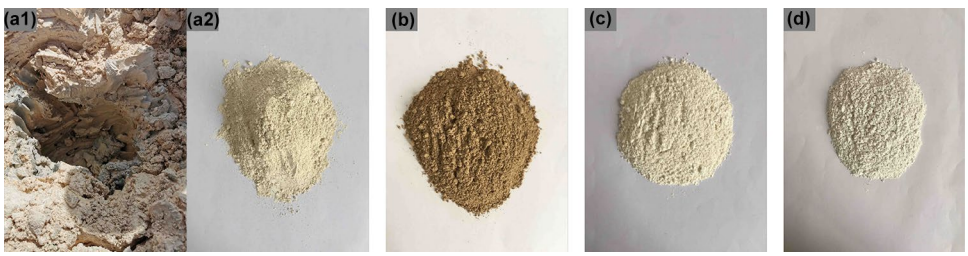

Fig. 3 Contrast of different soil samples: **a1** Coral clay field status; **a2** Coral clay **b** Chongqing silt; **c** Kaolin; **d** Talcum

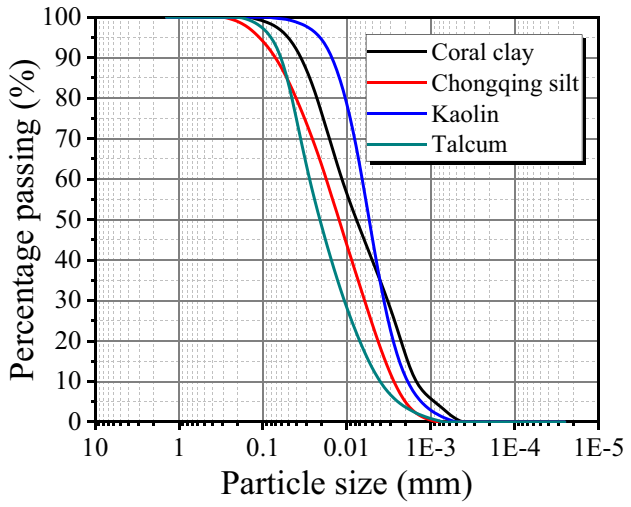

Fig. 5 Cumulative curve of particle size distribution of different soils

Furthermore, the curvature coefficient (C_c) is an index to quantify whether the slope of the cumulative curve of soil particle gradation is continuous or not (Knappett and Craig 2012). The specific definition is as follows:

$$C_u = d_{60}/d_{10} \tag{1}$$

$$C_c = \frac{{d_{30}}^2}{d_{60} \times d_{10}} \tag{2}$$

Among them, where d_{10} is the effective particle size, d_{30} is the particle size where the mass of soil particles smaller than this size accounts for 30% of the total mass of the soil particles, d_{60} is the controlled particle size.

It can be seen from Table 2 that the uneven coefficient $C_u > 5$ of coral clay and Chongqing silt can be judged to be uneven soil. Furthermore, the gradation curve is discontinuous as $C_c < 1$; therefore, it is determined that coral clay and Chongqing silt are poor gradation. It is suggested that kaolin is homogeneous soil because of its uneven coefficient $C_u < 5$. Moreover, the gradation curve is continuous as $1 < C_c < 3$; hence, it is also determined that kaolin has a poor gradation. It is assumed that talcum is uneven soil according to the uneven coefficient $C_u > 5$. Besides, the gradation curve is continuous as $1 < C_c < 3$. Therefore, it is determined that the talcum has a good gradation.

The size, shape, mutual arrangement and connection of soil particles have an important influence on the structure of soil. We conducted microscopic experiments with Quattro S scanning electron microscope and obtained the microscopic morphology of different soils in a naturally dry and loose state, as well as the structural forms of different soils, as shown in Fig. 6.

It can be seen in Fig. 6(a) that the coral clay particles, with a large particle size span, have different morphologies. There are a large number of flake clay particles, the very fine strip and needle-shaped particles distributed on the surface of the large particles. Among them, these irregular flake clay particles are stacked together. It can be seen in Fig. 6(b) that the microscopic particle size and shape of Chongqing silt are different, and the morphological distribution is more complicated. Part of it shows face-to-face flaky accumulation, forming a scattered structure, and some irregular soil fragments are stacked together. The particles are combined via different ways to form micropores of different shapes. As can be seen in Fig. 6(c), kaolin particles are mostly in the form of flakes and are stacked into clusters of different sizes. It can be seen in Fig. 6(d) that the microscopic particle size and shape of the talcum are different. The surface of the large particles is distributed with flake particles, and some flake particles are stacked together to form clusters of different shapes.

In order to obtain mineral types and content of coral clay and Chongqing silt, D8 ADVANCE X-ray diffractometer was used to analyze the mineral composition of coral clay and Chongqing silt. The mineral composition was identified according to the element types obtained in the XRF test (as shown in Table 3), and the diffraction peak shape, intensity as well as d value in the XRD test results. In this paper, the MID Jade software was used to analyze the diffraction patterns of coral clay and Chongqing silt. In order to get the main mineral composition of coral clay and Chongqing silt, the diffraction patterns were obtained from the XRD test of coral clay and Chongqing silt, which were compared and fitted with the PDF standard card in the phase retrieval library ICDD. Then the RIR method was used to calculate the mineral content of a variety of mineral components in coral clay and Chongqing silt. The test results are shown in Fig. 7 and Table 4.

It is concluded that the main chemical composition of coral clay is $CaCO_3$, and the main mineral composition is Aragonite, Calcite and Calcite magnesian. The percentage of each mineral composition accounts for 39.5%, 35.5% and 25%, respectively. The main mineral components of Chongqing silt are Quartz (SiO_2), light mica Alurgite 2M1($(K_{.94}Na_{.06})(Mg_{.08}Al_{1.75}Fe_{.15}Mn_{.02})(Al_{.92}Si_{3.08})O_{10}(OH)_2$), Clinochlore 2 M ($Al_2Mg_5Si_3O_{10}(OH)_8$) and Albite, Ca-rich, ordered ($(Na,Ca)Al(Si,Al)_3O_8$). And the content is 12.2%, 19.3%, 61.9% and 6.6%, respectively. The crystalline chemical formula of kaolin is $Al_2O_3{\cdot}2SiO_2{\cdot}2H_2O$. The chemical name of talcum is hydrated magnesium metasilicate, whose molecular formula is $Mg_3Si_4O_{10}(OH)_2$. Due to the high purity of kaolin and talcum, XRD diffraction test about these is not carried out.

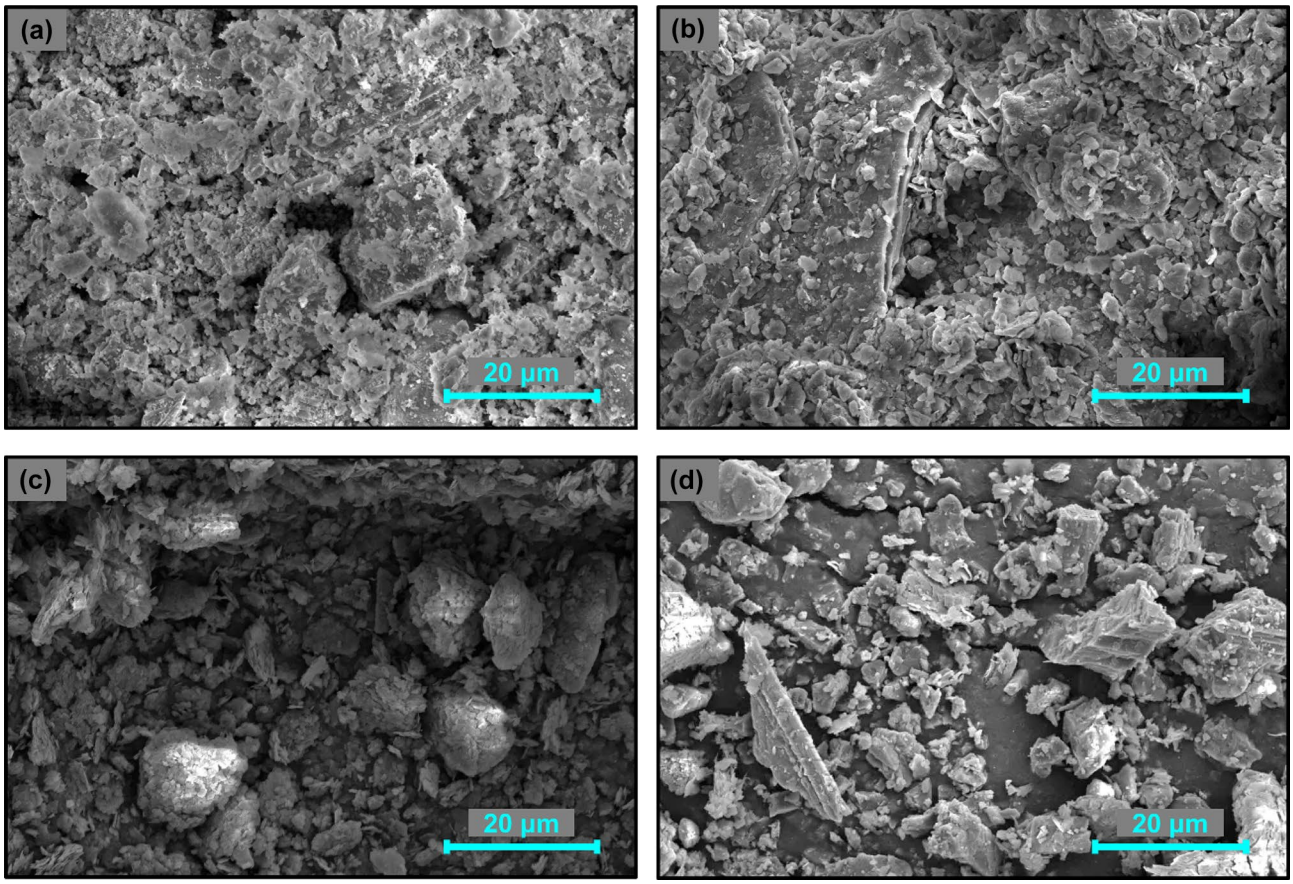

Fig. 6 The microscopic morphology of different soils: **a** Coral clay; **b** Chongqing silt; **c** Kaolin; **d** Talcum

Experiment method

Coral clay and Chongqing silt were air-dried and crushed, and then passed through a 2-mm sieve. In contrast, the purchased kaolin and talcum have fine particle size and do not need to be processed. The four soil samples were placed in different containers, mixed with pure water to prepare a slurry with the same moisture content. The slurry was stirred with an H2025G electric mixer until the slurry was evenly stirred with no bubbles. In order to make the mud deposition reach a stable state, the surfaces of the prepared four mud liquid containers were sealed with plastic wrap and left standing for 24 h. The floating water on the surface of the samples in each container was sucked away, and the soil samples were poured into a rectangular plexiglass container with an inner diameter of 20 cm × 20 cm × 5 cm. In order to study the influence of the layer thickness on the desiccation cracking, the control layer thickness of each soil sample was set as 5 mm, 10 mm, and 15 mm, respectively. And a total of 12 samples were configured in the experiment. The specific test program is shown in Table 5. The prepared samples being placed in an oven set to 30 ℃ were dried at a constant temperature. When the quality of the samples were not changing, the drying process ends. Then the dried samples were taken out. Subsequently, the Nikon D810 camera was used to photograph the soil surface morphology. For the purpose of adjusting the appropriate height between the camera and the sample, a level was used to correct and fix the camera's verticality. Besides, the incandescent lamp was used for light adjustment so that the light source on the surface of the sample is uniform during the shooting.

Image processing and crack quantification

In order to reduce the influence of container boundary on the soil surface cracking, the middle part of the sample (size 18 cm × 18 cm) was selected for quantitative analysis. Firstly, Image processing softwares, such as Photoshop, Image J and other software, were used for preprocessing, cutting and size correction of the image, and then MATLAB programming was use for grayscale, denoising and binarization of the image. Finally, Pore and Crack Image Analysis System (PCAS) software developed by (Liu et al. 2013) was used to analyze and obtain the parameters of the image. Figure 8 shows the specific process of image processing.

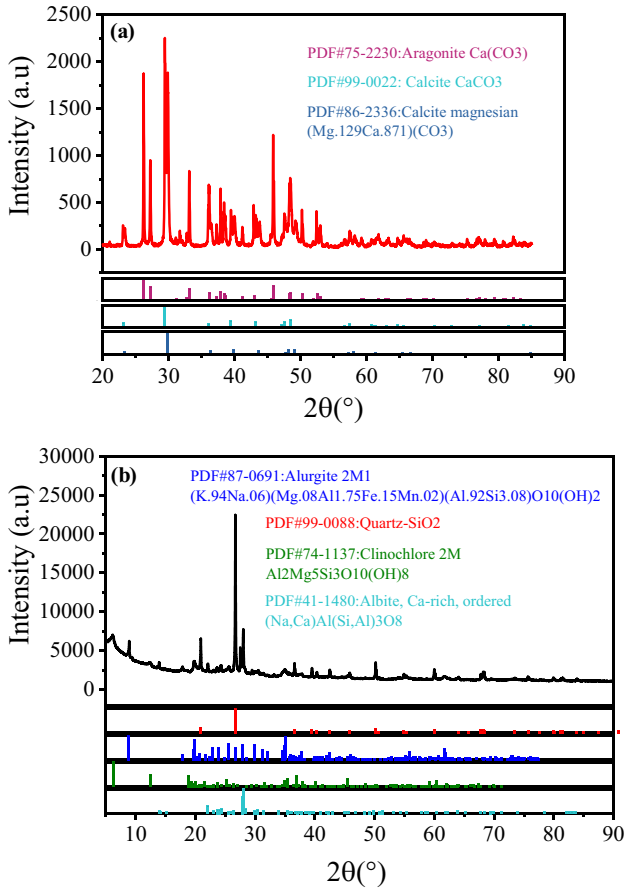

Fig. 7 Diffraction pattern: **a** Coral clay; **b** Chongqing silt

Using PCAS software, we can obtain the relevant crack parameters, including number of nodes, number of crack segments, total crack area, surface crack rate, total length of cracks, average length of cracks and average width of cracks. Meanwhile, the relevant clod parameters can also be obtained, including number of clods, total area of clods, average area of clods, and maximum area of clods. The geometric parameters of the sample, namely fractal dimension, can also be obtained.

The unit of the relevant parameters obtained by the image processing software is the pixel. The actual size of the sample is proportional to image pixel size. In this paper, the relevant crack parameters (total crack area, total length of cracks, average length of cracks and average width of cracks) and clod parameters (total area of clods, average area of clods, and maximum area of clods) were converted into actual size. The conversion method is as follows,

$$L_i = \mu L_i^{'} \tag{3}$$

$$A_i = \lambda A_i^{'} \tag{4}$$

where $L_i^{'}$ and $A_i^{'}$ are the pixel length and pixel area obtained by the image processing software, respectively. L_i and A_i are the actual length and actual area of the sample, respectively. μ and λ are the sample length conversion coefficient and area conversion coefficient, respectively, and they have the following relationship.

$$\mu = \sqrt{\lambda} \tag{5}$$

where λ is defined as the ratio between the actual area A_I of the sample and the pixel area $A_i^{'}$ of the sample, namely

$$\lambda = A_I / A_I^{'} \tag{6}$$

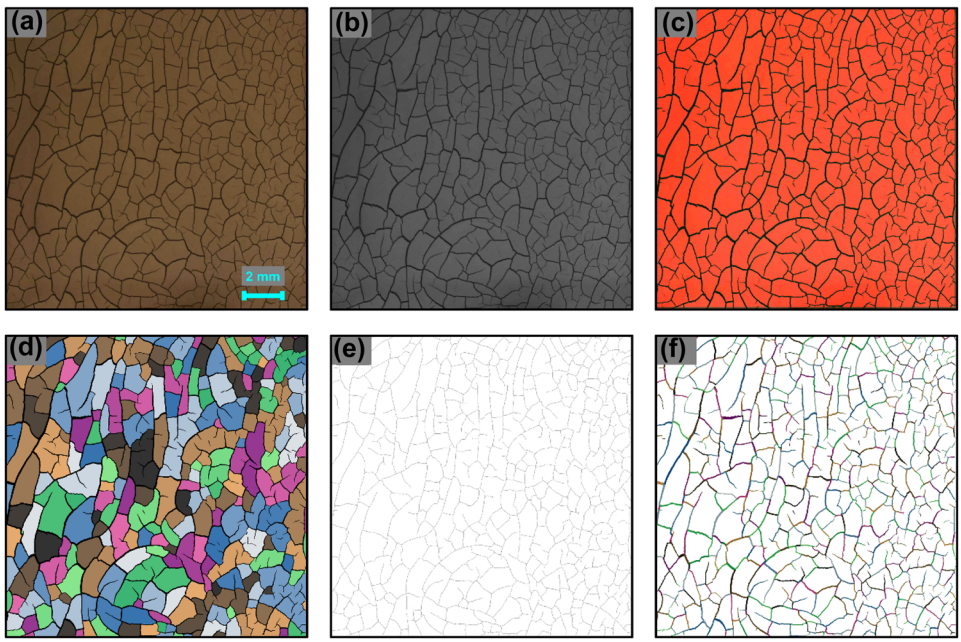

Fig. 8 Image processing procedures

Using the above formulas, the actual size of the relevant crack parameters and clod parameters were obtained.

Crack-related parameters: Number of nodes is defined as the total number of cracks between two adjacent nodes. Total crack area, that is, the sum of all crack areas of the sample. Surface crack rate refers to the rate of crack area to total area of the sample, which reflects the degree of cracking to a certain extent. Total length of cracks, i.e., the total length of the center line of crack skeleton network. Average length of cracks reflects an indicator of the central tendency of crack length. Average width of cracks reflects an indicator of the central tendency of crack width. In this paper, surface crack ratio is a basic crack parameter, which is defined as the ratio of the total crack area to the total area of clods, namely:

$$C_r = A_{crack}/A_{clod} \tag{7}$$

There exists the following relationship between surface crack rate and surface crack ratio.

$$C_n = \frac{C_r}{1 + C_r} \times 100\% \tag{8}$$

where C_r is the surface crack ratio, C_n is the surface crack rate, A_{crack} is the total area of the cracks, and A_{sclod} is the total area of the soil clod.

Clod-related parameters: Number of clods is an indicator that reflects the extent to which the soil is divided by cracks. Total area of clods refers to the sum of the area of all the clods. Average area of clods reflects an indicator of the central tendency of the clods divided by the cracks. Maximum area of clods refers to the soil clod area with the largest proportion of the plane space in the clods divided by all cracks.

Fractals are common in the nature, such as clouds, ice crystals, snowflakes, rivers, mountains, coastlines, patterns of plant and animal fur, etc. Likewise, soil cracks also have statistically self-similar fractal characteristics. Based on the law of statistical distribution, the box dimension method is adopted to calculate the fractal dimension of the crack network of different scales of soil. Initially, soil crack network is divided into a grid with side length ε_i (i is an even multiple of the pixel), then the number of corresponding geometric bodies with self-similarity is determined. Ultimately, to get the following linear relationship, the obtained data are fitted in the rectangular coordinate system.

$$\lg N(\varepsilon_i) = A - D\lg \varepsilon_i \tag{9}$$

where A is a constant and D is the value of the fractal dimension reflecting the shape of the crack. The value of fractal dimension is shown in Table 6.

Results and analysis

Crack morphology

Figures 9 and 10 show the final morphology of each sample. From the figure, we can see that coral clay, Chongqing silt and talcum of different layer thickness and temperature all present a significant crack network. And as the layer thickness increases, the area of the clods divided by the cracks increases. On the contrary, the number of clods decreases. However, due to the high consistency of kaolin, it is difficult for all the fine bubbles to be discharged. "Y" and "1" shaped tiny cracks occur at the defects formed on the surface of these pores, but the tiny cracks formed have not propagated. Kaolin with a thickness of 10 mm not only forms tiny cracks at the pore defects, but also forms a few cracks perpendicular to the container wall. It can be concluded that kaolin has better crack resistance than coral clay, Chongqing silt and talcum. It can also be seen that the cracks all present three-pronged intersection forms such as "T" and "Y" shapes. The intersection angle of the cracks is mostly 90°. The shapes of the soil clods divided by the cracks are different, and most of them are triangles, polygons, ellipses, and fans.

Crack parameters analysis

The soil crack can be measured by crack indicators that affect its physical and mechanical properties, i.e., number of nodes, number of crack segments, total crack area, surface crack rate, total length of cracks, average length of cracks, average width of cracks, and surface crack ratio. Through the analysis of the data obtained by image processing, the relationship curve between each crack parameter and different soil layer thickness and temperature is obtained, as shown in Figs. 11 and 12.

The number of nodes is an important parameter reflecting the degree of fragmentation of soil, which includes the number of crack end nodes and cross nodes. It can be seen from Fig. 11(a) that, in general, the number of nodes decreases as the layer thickness of the soil sample increases. In the case of a lower layer thickness, the samples all have a higher number of nodes. The number of nodes of coral clay and Chongqing silt under each layer thickness is higher than that of talcum under corresponding layer thickness. The number of nodes of talcum is less affected by the layer thickness. As the layer thickness increases, the number of nodes, with a little change, first decreases slightly, and then increases slightly. The number of nodes in Chongqing silt with a layer thickness of

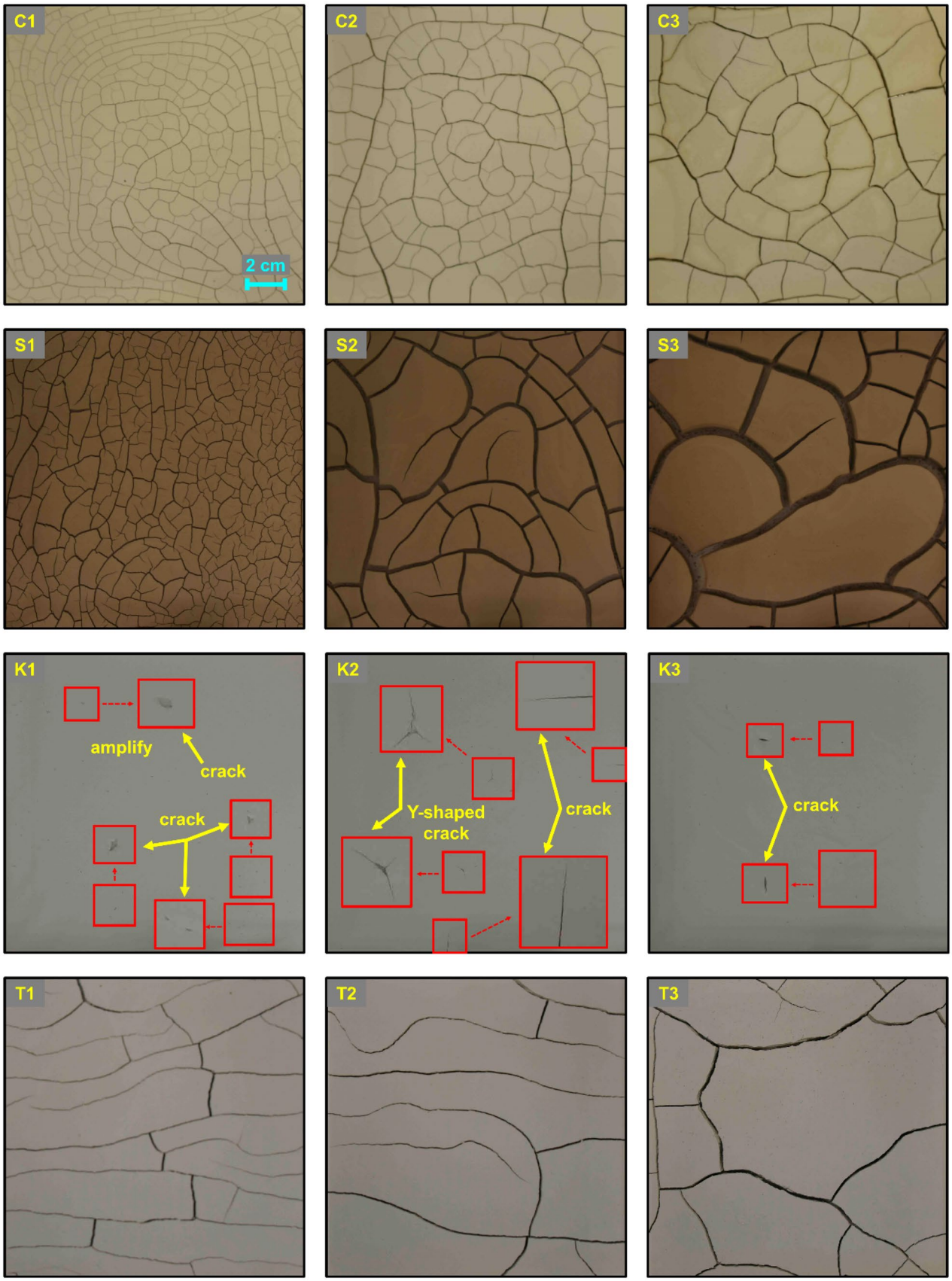

Fig. 9 Comparison of final desiccation cracks under different layer thicknesses

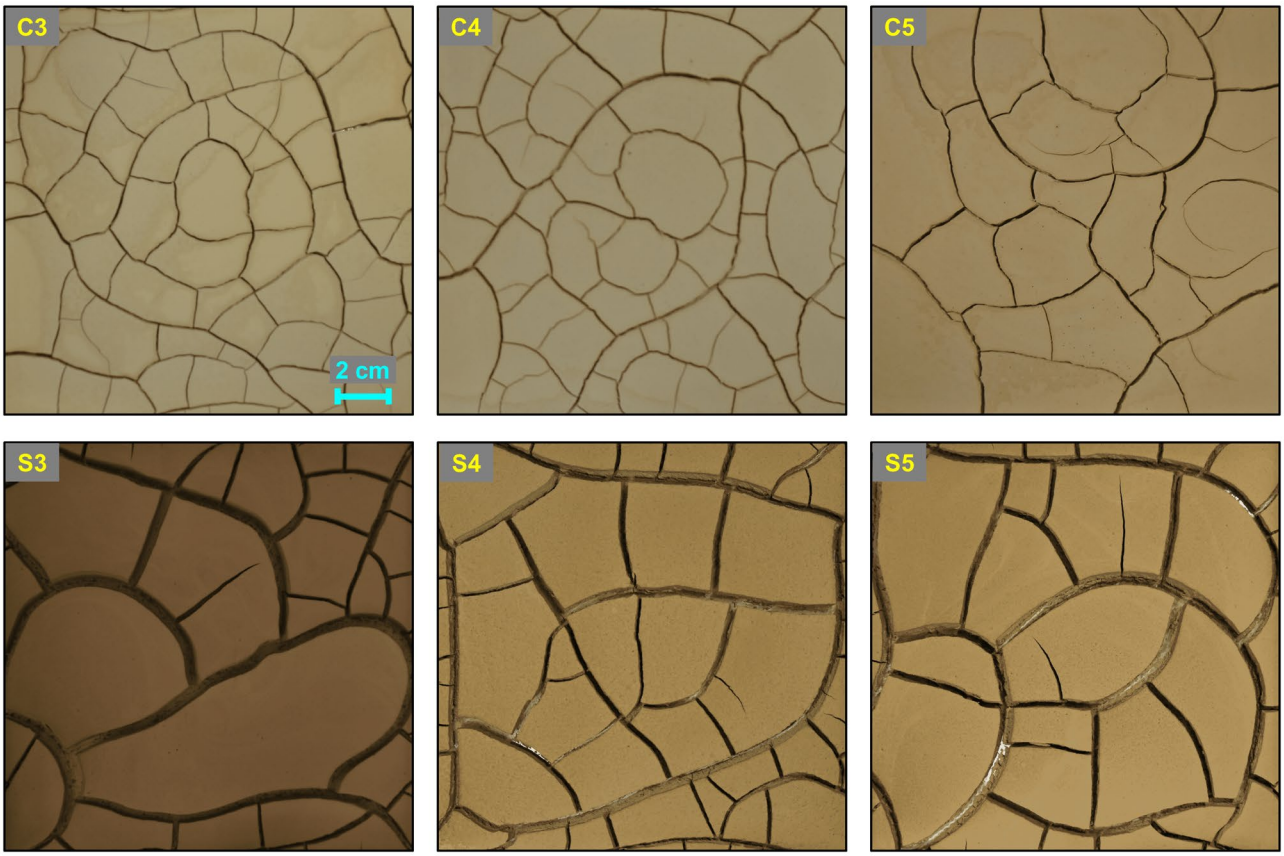

Fig. 10 Comparison of final desiccation cracks under different temperatures

5 mm is greater than that of coral clay and talcum with corresponding layer thickness. The number of nodes of coral clay with layer thickness of 10 mm and 15 mm is greater than that of Chongqing silt and talcum with corresponding thickness. It can be seen from Fig. 11(b) that the changing law between the number of crack segments and the layer thickness is more consistent with the changing law of the number of nodes, but the number of crack segments between coral clay with a layer thickness of 5 mm and Chongqing silt with corresponding layer thickness is relatively close. It can be seen in Fig. 11(e) that the total length of cracks decreases with the increase of the layer thickness. For coral clay, there is a good linear relationship between the total length of cracks and the layer thickness; the total length of cracks of Chongqing silt decreases significantly first with the increase of the layer thickness, and then decreases slowly. However, the total length of cracks of talcum decreases slowly with the increment of the layer thickness. Due to the different types of soil, the laws presented are different. It can be observed in Fig. 11(c), (h), (d) that the crack parameters, i.e., the total crack area, the surface crack rate and the surface crack ratio, are consistent with the rules of layer thickness. These crack parameters of coral clay decrease with the increment of layer thickness, while these crack parameters of Chongqing silt show the opposite trend. For the parameters of talcum, it decreases first and then increases as the layer thickness increases. In Fig. 11(f), the average length of cracks of coral clay and Chongqing silt both show a linear increasing trend with the increment of layer thickness, while the average length of cracks of talcum increases first and then decreases significantly with the increment of layer thickness. Among them, when the layer thickness is 5 mm, coral clay and Chongqing silt have a similar average length of cracks, and when the layer thickness is 15 mm, Chongqing silt and talcum have a similar average length of cracks. In Fig. 11(g), the average width of cracks for each type soil increases with the increment of layer thickness and shows a good linear relationship. Among them, the average width of cracks about coral clay and talcum both increase slowly with the increment of layer thickness, while the average width of cracks about Chongqing silt increases significantly with the increase of layer thickness.

The effect of temperature on the crack parameters of coral clay and Chongqing silt is obviously different (Fig. 12). It can be seen from Fig. 12(a), (b), (e) that with the increase

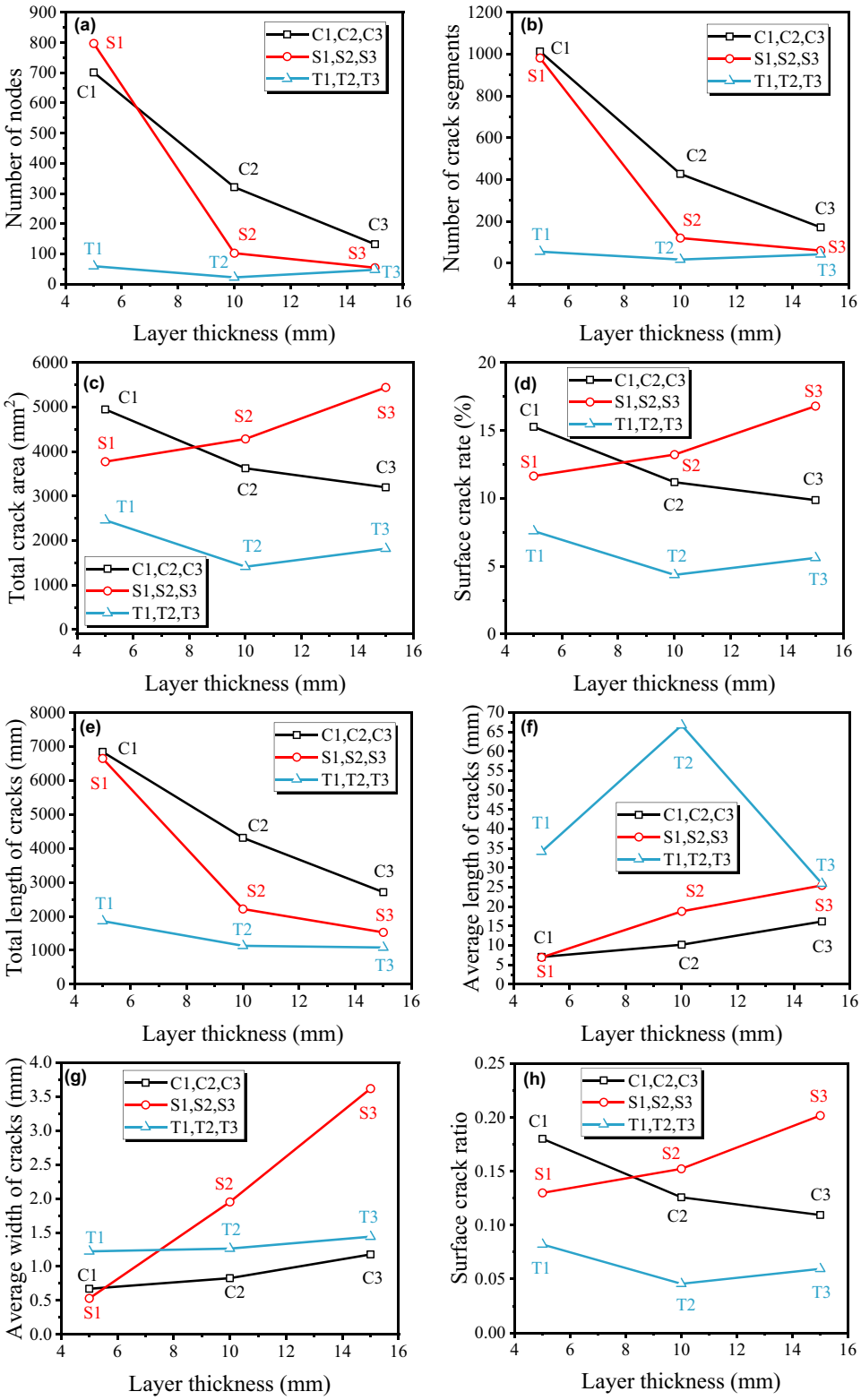

Fig. 11 The relationship curve between crack index and layer thickness: **a** Number of nodes; **b** Number of crack segments; **c** Total crack area; **d** Surface crack rate; **e** Total length of cracks; **f** Average length of cracks; **g** Average width of cracks; **h** Surface crack ratio

of temperature, number of nodes, number of crack segments and total length of cracks of coral clay decrease, while these of Chongqing silt show increase first and then decrease. Figure 12(c), (d) and (h) can be observed that the total crack area, surface crack rate and surface crack ratio of coral clay all show a decreasing trend with the increase of temperature, while those of Chongqing silt show an increasing trend. The average length of cracks of coral clay and Chongqing silt both decrease

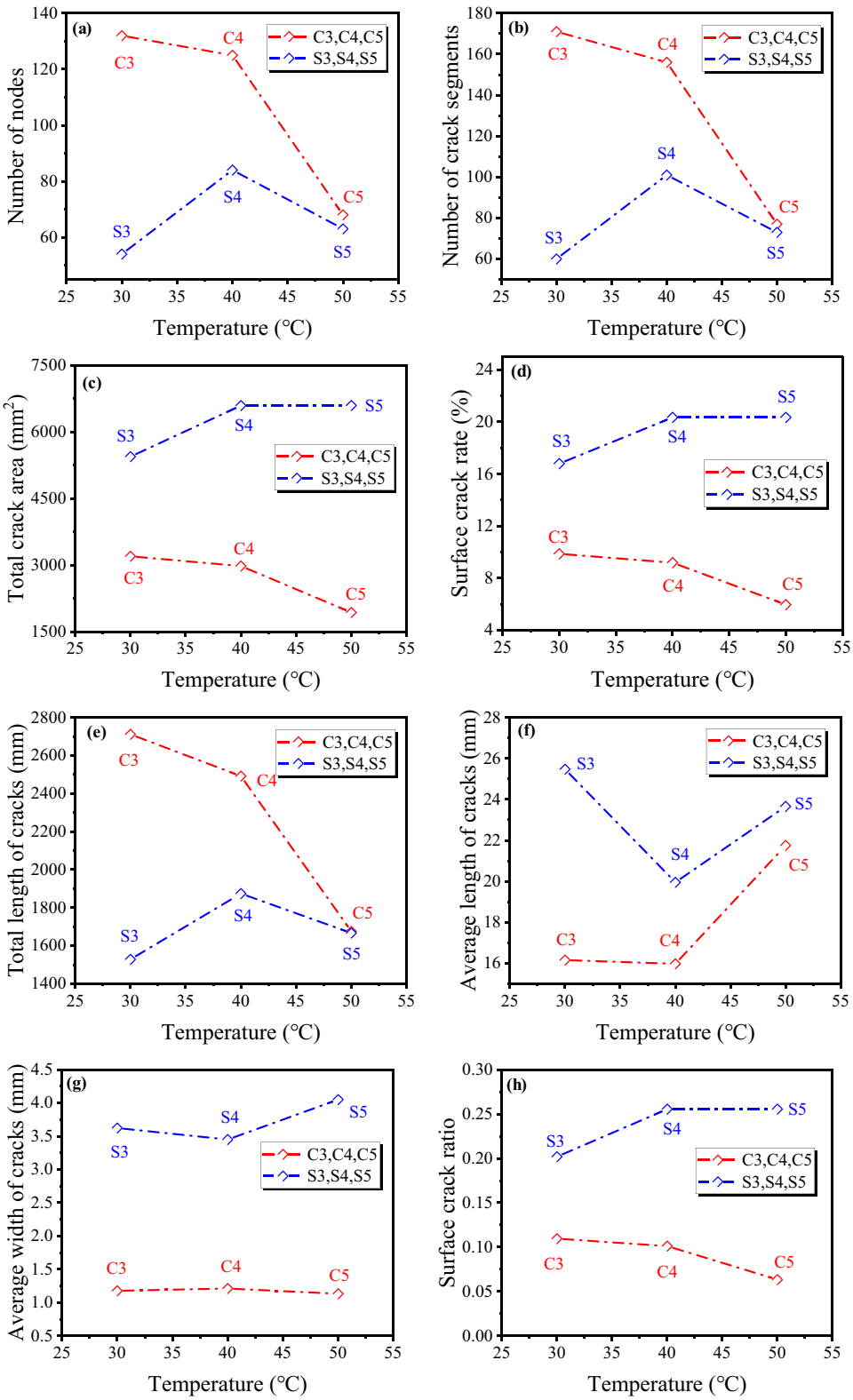

Fig. 12 The relationship curve between crack index and temperature: **a** Number of nodes; **b** Number of crack segments; **c** Total crack area; **d** Surface crack rate; **e** Total length of cracks; **f** Average length of cracks; **g** Average width of cracks; **h** Surface crack ratio

first and then increase with increasing temperature (Fig. 12(f)). Moreover, the average width of cracks of coral clay varies slightly with the increase of temperature, while Chongqing silt shows a slight decrease at first and then increase.

Surface crack rate refers to the ratio of total crack area to the total area of the soil. The total area of the soil changes little and can be considered as a fixed value. Therefore, the surface crack rate is positively correlated with the total crack

area. It can be seen from Fig. 11(c) that with the increase of layer thickness, the total crack area of Chongqing silt gradually increases, while the coral clay decreases. Therefore, the surface crack rates of coral clay and Chongqing silt also show this opposite law. Total crack area approximately equal to total length of cracks multiplied by average width of cracks. It can be seen from Fig. 11(e) that the total length of cracks of Chongqing silt and coral clay decrease with the increase of layer thickness, while the average width of cracks increase with the increase of layer thickness. The increase of average width of cracks of coral clay is smaller; while the Chongqing silt has a more significant increase (Figs. 9 and 11(g)), which contributes more to the total crack area. This results in an increase of the total crack area, which in turn leads to an increase in the surface crack rate. From this aspect, the reason for this opposite law can also be explained. Meanwhile, it can also be seen that Chongqing silt has greater shrinkage than coral clay, resulting in a more significant increase in the average width of cracks of Chongqing silt. It also shows that different soils, due to different structures and mineral compositions, will lead to significant differences in the desiccation cracking characteristics of different soils.

Clod parameters analysis

The clods divided by the soil cracks can be measured by the clod parameters, i.e., number of clods, total area of clods, average area of clods and maximum area of clods, which affect its physical and mechanical properties. By analyzing the data obtained by image processing, the relationship curve between each clod parameter and different layer thickness was obtained, as shown in Fig. 13. It can be seen from Fig. 13(a) that the number of clods about coral clay of each layer thickness is greater than Chongqing silt at corresponding layer thickness, and the number of clods about Chongqing silt is greater than talcum with corresponding layer thickness. When the layer thickness is less than 10 mm, the number of clods about coral clay and Chongqing silt decreases significantly with the increase of

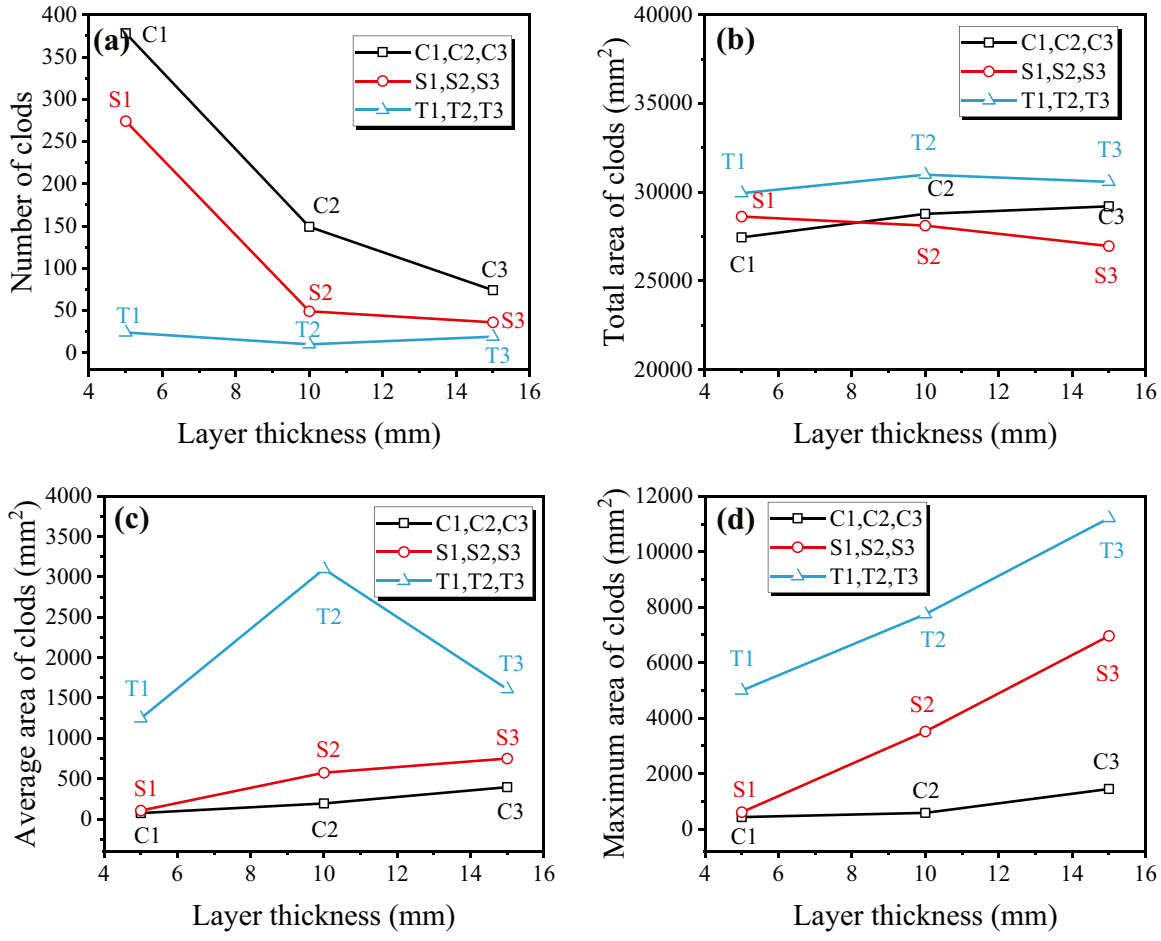

Fig. 13 The relationship curve between clod index and layer thickness: **a** Number of clods; **b** Total area of clods; **c** Average area of clods; **d** Maximum area of clods

the layer thickness. Meanwhile, when the layer thickness is greater than 10 mm, the degree of decline slows down. It can be seen that coral clay and Chongqing silt have relatively consistent changes between the number of clods and layer thickness. The number of clods about talcum is generally small. As the layer thickness increases, the number of clods about talcum slowly decreases first and then slowly increases. It can be seen from Fig. 13(b) that the total area of clods about coral clay slowly increases with the increment of layer thickness. Chongqing silt showed the opposite law, i.e., the total area of clods about Chongqing silt decreased slowly with the increase of layer thickness, and both showed a good linear relationship. The total area of clods about talcum has changes a little, which increases slowly first with the increase of layer thickness, and then decreases slowly. It can be seen from Fig. 13(c) that the average area of clods about coral clay and Chongqing silt fluctuates relatively little with the change of layer thickness, and the parameter increases linearly and slowly with the increase of layer thickness. As for talcum, the parameter increases significantly first as the layer thickness increases, and then decreases significantly. It can be observed from Fig. 13(d) that the maximum area of clods about coral clay, Chongqing silt and talcum all show a linear increase trend with the increase of layer thickness. And the maximum area of clods about Chongqing silt and talcum increases significantly with the increment of layer thickness. For the maximum area of clods about coral clay, it increases slowly with the increment of the layer thickness. In general, talcum has the larger maximum area of clods value under the conditions of each layer thickness, followed by Chongqing silt and coral clay.

With the increase of temperature, number of clods of coral clay decreases, while Chongqing silt increases first and then decreases (Fig. 14(a)). The total area of clods of coral clay increases slightly with the increase of temperature, while Chongqing silt shows the opposite trend (Fig. 14(b)). Average area of clods of coral clay increases with the increase of temperature, while Chongqing silt shows first decrease and then increase (Fig. 14(c)). With the increase of temperature, maximum area of clods of coral clay increases slightly, while Chongqing silt shows a significant decrease at first and then a slight increase (Fig. 14(d)). The effect of temperature is mainly reflected in promoting the earlier, faster propagation and stability of cracks, and the influence law on the final parameters is relatively insignificant (Luo et al. 2020; Fang et al. 2021).

Morphological analysis of fractal dimension

The fractal dimension is often used to reflect the distribution of cracks on the soil surface. It can be seen from Fig. 15(a) that the fractal dimensions of coral clay, Chongqing silt and talcum all increase with the increment of layer thickness. Moreover, in coral clay and talcum, there is a good linear relationship between the fractal dimension and the layer

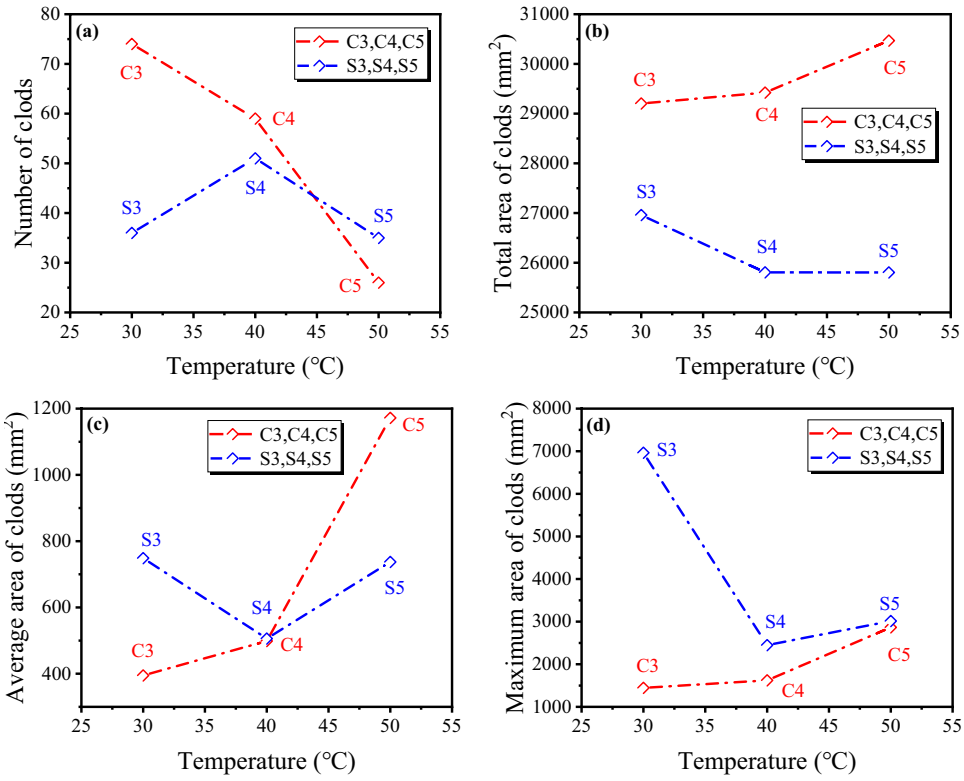

Fig. 14 The relationship curve between clod index and temperature: **a** Number of clods; **b** Total area of clods; **c** Average area of clods; **d** Maximum area of clods

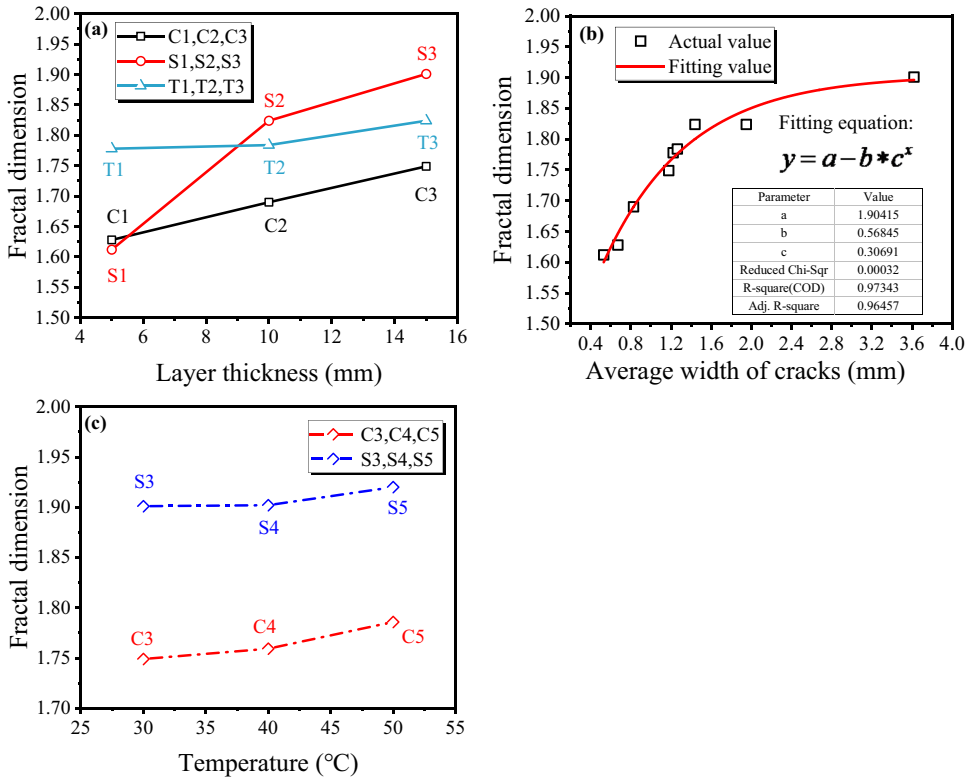

Fig. 15 Fractal dimension: **a** Layer thickness; **b** Average width of cracks; **c** Temperature

thickness. While the fractal dimension of Chongqing silt increases significantly at first and then increases slowly with the increment of the layer thickness. Figure 15(c) shows that fractal dimensions of coral clay and Chongqing silt both increase slowly with the increase of temperature.

The average width of cracks is an important parameter affecting the fractal dimension. The size of the average width of cracks will significantly affect the degree of self-similarity of the cracks on the soil surface, thereby affecting the change law of the fractal dimension. Therefore, it is necessary to reveal the relationship between the average width of cracks and the fractal dimension. From Fig. 15(b), it can be concluded that there is an exponential relationship between the fractal dimension and the average width of cracks. There is a high degree of agreement between the actual value and the fitted value. The fitting function is:

$$y = a - b * c^{x} \tag{10}$$

where y is fractal dimension, x is average width of cracks. Moreover, a = 1.90415, b = 0.56845, c = 0.30691, and $R^2 = 0.96457$.

Analysis of crack morphological distribution

The layer thickness affects the morphological distribution of soil cracks. In order to explore the effect of layer thickness on the morphological distribution characteristics of cracks, a statistical analysis was carried out on the crack length, crack width, clod area and crack direction. Figure 16 shows the frequency distribution of the crack length; Fig. 17 shows the frequency distribution of the crack width; Fig. 18 shows the frequency distribution of the clod area; Fig. 19 shows the frequency distribution of the crack direction.

It can be seen from Fig. 16(a), (b) that the distribution range of the crack length about coral clay and Chongqing silt gradually expands with the increment of layer thickness, i.e., C3 > C2 > C1, S3 > S2 > S1. The distribution range of crack length about talcum shows a trend of increasing first and then decreasing with the increment of layer thickness, i.e., T2 > T1 > T3. And the crack length distribution of T2 and T3 is discontinuous. For instance, T2 has a missing distribution between 60 and 120 mm in length, and T3 has a missing distribution between 60 and 90 mm in length. Under a certain layer thickness, the distribution range of the crack length of different soils varies greatly. For instance, when the layer thickness is 5 mm, the crack length distribution ranges of C1, S1, and T1 are 0 ~ 25.00 mm, 0 ~ 31.50 mm and 0 ~ 120.00 mm, respectively; When the layer thickness is 10 mm, that of C2, S2 and T2 are 3.50 ~ 27.50 mm, 0 ~ 56.00 mm and 0 ~ 195.00 mm, respectively; when the layer thickness is 15 mm, that of C3, S3 and T3 are 2.50 ~ 45.00 mm, 7.00 ~ 70.00 mm and 0 ~ 105.00 mm, respectively. The maximum relative frequency of the crack length of C1, C2, and C3 are 0.37, 0.21, and 0.13,

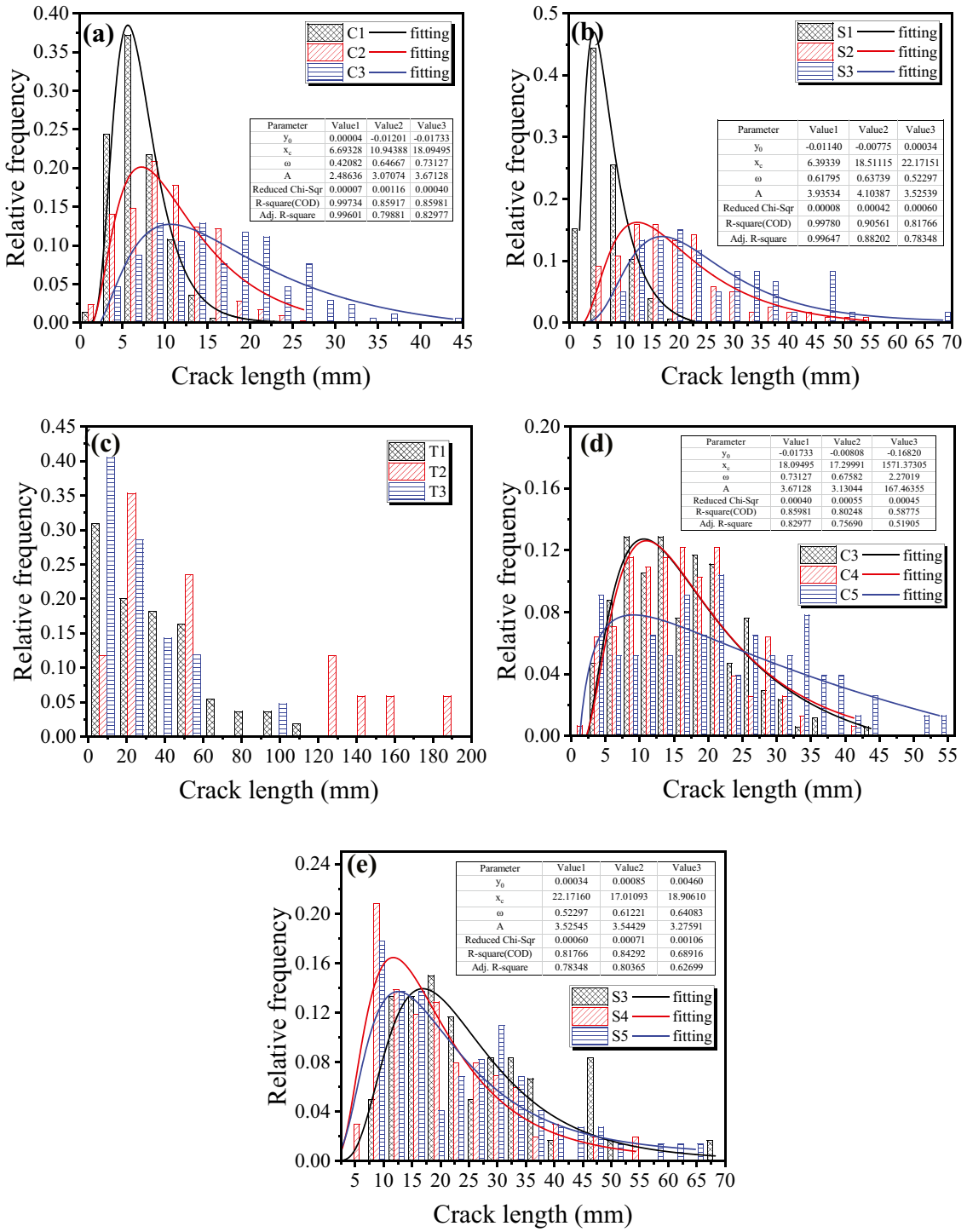

Fig. 16 Frequency distribution of the crack length

respectively, and that of S1, S2, and S3 are 0.44, 0.16, and 0.13, respectively, while that of T1, T2, and T3 is 0.30, 0.35 and 0.40, respectively. It was found that the maximum relative frequency of the crack length about coral clay and Chongqing silt decreased significantly with the increment of the layer thickness, while that of talcum showed the opposite law. However, the maximum relative frequency values of the crack length are relatively close (Fig. 16(c)).

Through the fitting analysis of the frequency distribution of the crack length, it is found that the crack length distribution of talcum is discontinuous and the fitting effect is poor, while the fitting effect of the frequency distribution of

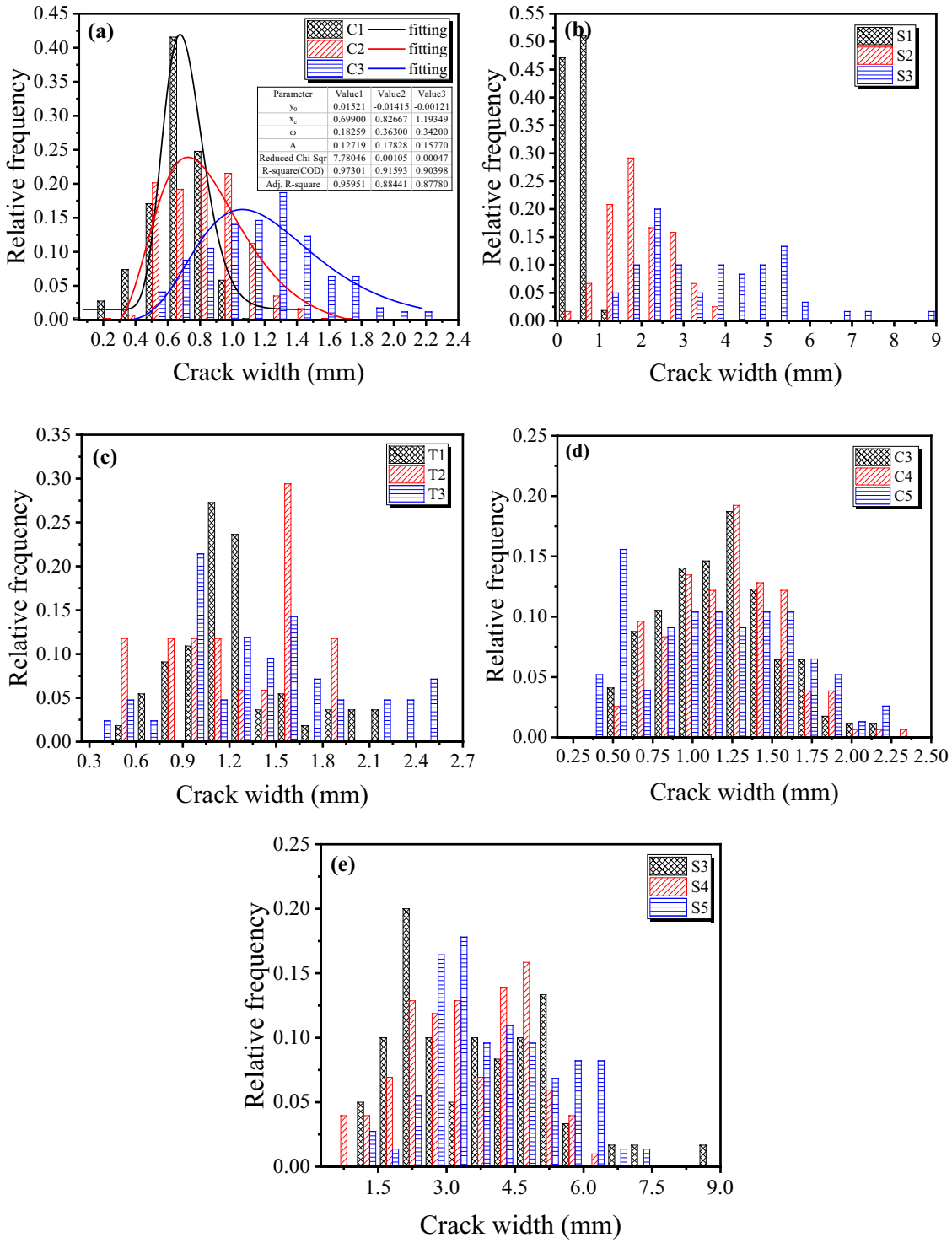

Fig. 17 Frequency distribution of the crack width

the crack length about coral clay and Chongqing silt under different layer thickness and temperature conditions is relatively better, which conforms to the form of LogNormal function curve, as follows:

$$y = y_0 + \frac{A}{\sqrt{2\pi\omega x}} e^{\frac{-\left(ln\frac{x}{x_c}\right)^2}{2\omega^2}} \tag{11}$$

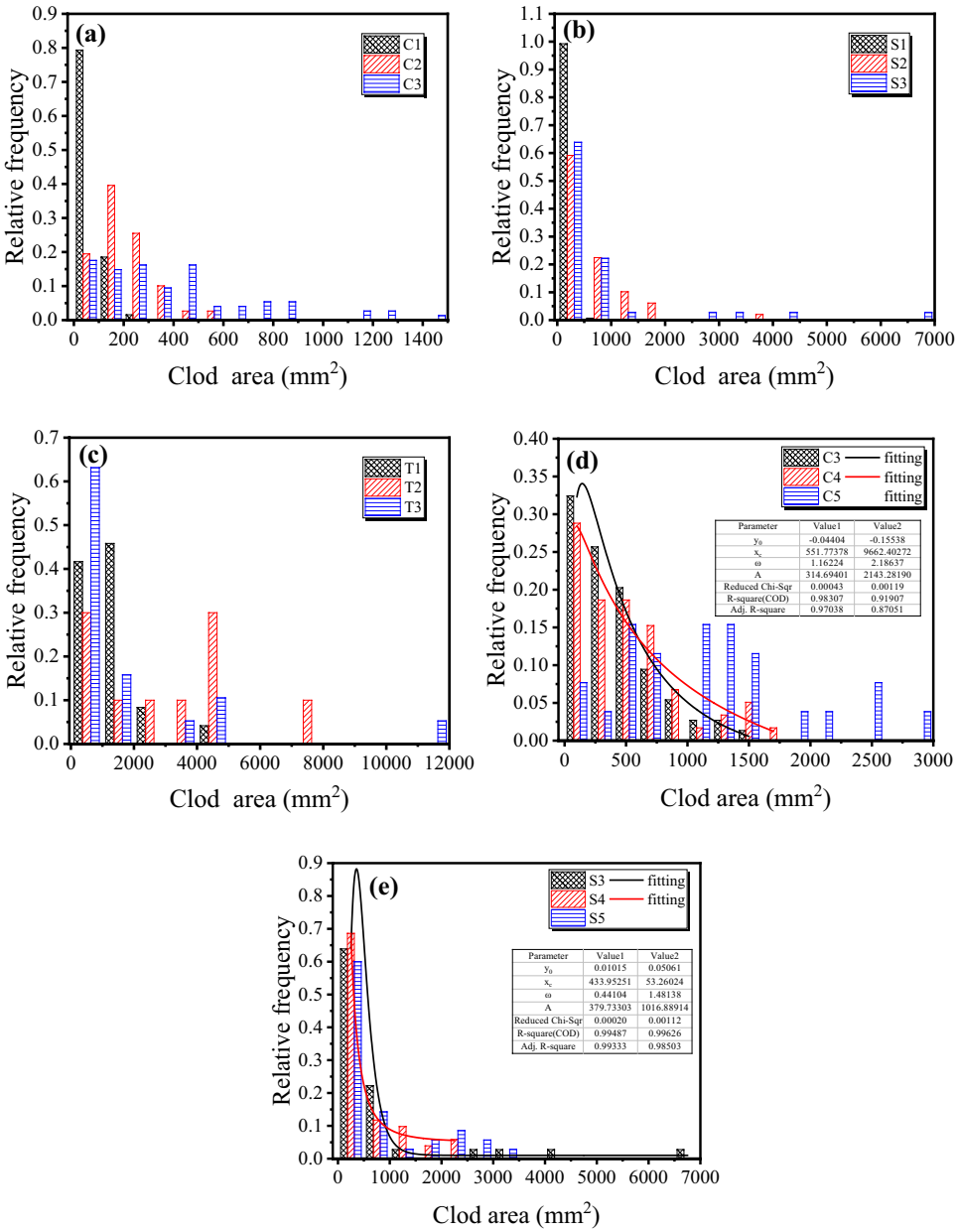

Fig. 18 Frequency distribution of the clod area

where y is relative frequency, and x is crack length. The specific values of the fitting parameters are shown in the tables in Fig. 16(a), (b), (d) and (e).

It can be seen from Fig. 17(a) and (b) that the distribution range of the crack width about coral clay and Chongqing silt gradually expands with the increment of layer thickness, i.e., C3 > C2 > C1, S3 > S2 > S1. It is similar to the crack length distribution of coral clay and Chongqing silt. The distribution range of the crack width about talcum showed a trend of decreasing first and then increasing with the increment of layer thickness, i.e., T3 > T1 > T2 (Fig. 17(c)). Under a certain layer thickness, the distribution range of the crack width about different soils varies greatly. For instance, when the layer thickness is 5 mm, the crack width distribution ranges of C1, S1, and T1 are 0 ~ 1.50 mm, 0 ~ 1.50 mm and 0.45 ~ 2.25 mm, respectively; when the layer thickness is 10 mm, that of C2, S2 and T2 are 0.15 ~ 1.80 mm, 0 ~ 4.00 mm, and 0.45 ~ 1.95 mm, respectively; when the layer thickness is 15 mm, that of C3, S3, and T3 are 0.45 ~ 2.25 mm, 1.00 ~ 9.00 mm and 0.30 ~ 2.55 mm, respectively. The maximum relative frequency of the crack width about C1, C2, and C3 are 0.42, 0.22, and 0.19, respectively, and that of S1, S2, and S3 are 0.45, 0.29, and 0.20, respectively, while that of T1, T2, and T3 is 0.27, 0.29 and 0.21, respectively. It is found that the maximum relative frequency of the crack width about coral clay and Chongqing silt decreased significantly with the increment of layer thickness, while that of talcum showed a trend of increasing first and

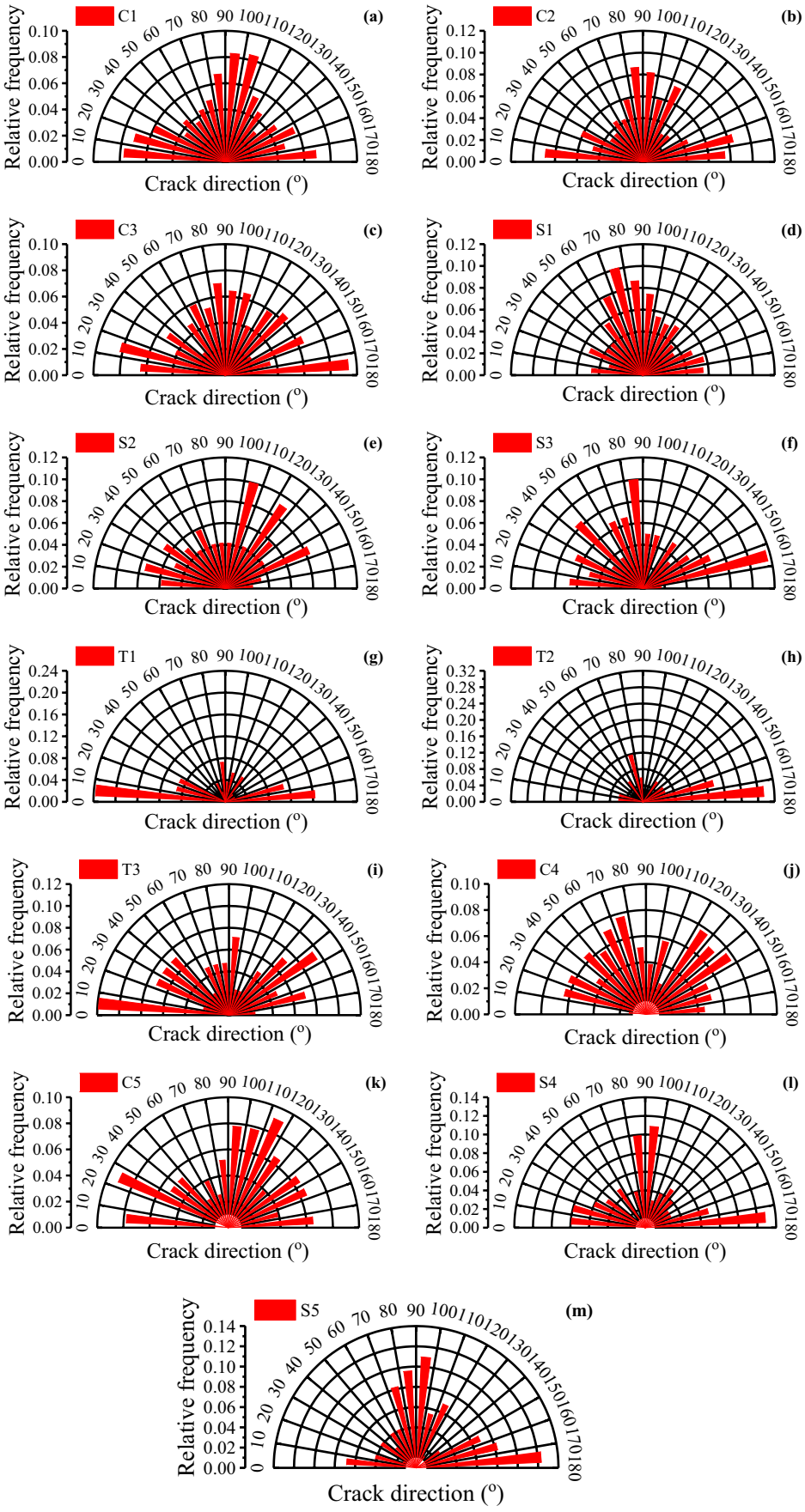

Fig. 19 Frequency distribution of the crack direction

then decreasing with the increment of layer thickness, but the maximum relative frequency values of the crack width are relatively close. Figure 17(d) and (e) shows that under different temperature conditions, the distribution range of crack width about coral clay is relatively close, while the crack width of Chongqing silt has a larger distribution range when the temperature is 30 °C.

Through the fitting analysis about the frequency distribution of the crack width, it is found that the fitting effect about the frequency distribution of the crack width about Chongqing silt and talcum is poor, while that of coral clay is better, which also conforms to the form of the LogNormal function curve. As shown in the formula (10), the specific values of each fitting parameter are shown in Fig. 17(a).

It can be seen from Fig. 18(a), (b) and (c) that the area distribution of various soil clods gradually expands with the increment of layer thickness, i.e., C3 > C2 > C1, S3 > S2 > S1 and T3 > T2 > T1. Under a certain layer thickness, the distribution range of the clod area about different soil varies greatly. For instance, when the layer thickness is 5 mm, the clod area distribution ranges of C1, S1, and T1 are 0 ~ 500 mm^2, 0 ~ 1000 mm^2, and 0 ~ 5000 mm^2, respectively; when the layer thickness is 10 mm, that of C2, S2, and T2 are 0 ~ 600 mm^2, 0 ~ 4000 mm^2 and 0 ~ 8000 mm^2, respectively; when the layer thickness is 15 mm, that of C3, S3 and T3 is 0 ~ 1500 mm^2, 0 ~ 7000 mm^2 and 0 ~ 12,000 mm^2, respectively. The maximum relative frequencies of the clod area about C1, C2, and C3 were 0.79, 0.40, and 0.18, respectively, and that of S1, S2, and S3 were 0.99, 0.59, and 0.64, respectively, while that of T1, T2 and T3 are 0.46, 0.30 and 0.63, respectively. It is found that the maximum relative frequency of the clod area about coral clay decreased significantly with the increment of the layer thickness, while that of Chongqing silt showed a significant decrease first and then a slight increase with the increase of the layer thickness. However, that of talcum decreases first and then increases significantly with the increment of layer thickness. When the layer thickness is small, the uniformity of the clod area finally formed by each soil is better. As the layer thickness increases, the soil clods divided by the cracks become larger. Besides, there are still some small soil clods, and the distribution range of the clod area is further expanded. At corresponding layer thickness, talcum has a larger clod area compared with coral clay and Chongqing silt. This phenomenon can also be seen in Fig. 9.

Figure 18(d) and (e) shows that with the increase of temperature, the distribution range of clod area about coral clay gradually increases, while the maximum relative frequency of clod area about Chongqing silt is relatively close, and distribution range of crack area is the largest when the temperature is 30 °C.

The direction of initiation and propagation of cracks affects the morphological distribution of cracks. Studying the distribution of crack angles can better describe the cracking phenomenon and understand the probability of choosing the direction of crack development.

It can be seen from Fig. 19 that the crack directions of C1 are mostly concentrated in 0° ~ 30°, 80 ~ 110°, and 150° ~ 180°, and the relative frequencies are 0.21, 0.23, and 0.17, respectively. The crack directions of C2 are mostly concentrated at 0° ~ 10°, 80 ~ 120°, and 160° ~ 180°, and the relative frequencies are 0.09, 0.30, and 0.16, respectively. The crack directions of C3 are mostly concentrated in 0° ~ 20°, 80 ~ 110° and 170° ~ 180°, and the relative frequencies are 0.15, 0.20 and 0.09, respectively. The crack directions of S1 are mostly concentrated in between 60° and 100°, and the relative frequency is 0.34.The crack directions of S2 are mostly concentrated in between 100° ~ 110°, 120° ~ 130° and 150° ~ 160°, and the relative frequencies are 0.10, 0.09 and 0.08, respectively. The crack directions of S3 are mostly concentrated in between 80° ~ 90° and 160° ~ 170°, and the relative frequencies are 0.10 and 0.12, respectively. The crack directions distribution in T1 and T2 are mostly horizontal. This phenomenon can also be observed in Fig. 9. The crack directions of T1 are mostly concentrated in between 0° ~ 10° and 170 ~ 180°, and the relative frequencies are 0.24 and 0.16, respectively. The crack directions of T2 are mostly concentrated in between 160 ~ 180°, and the relative frequency is 0.47. The crack directions of T3 are mostly concentrated at 0° ~ 10° and 140 ~ 150°, and the relative frequencies are 0.12 and 0.09, respectively. The crack directions of C4 are mostly distributed in 10° ~ 30°, 60° ~ 80° and 120° ~ 150°, and the relative frequencies are 0.13, 0.15 and 0.22, respectively. The crack directions of C5 are mostly distributed in 0° ~ 30°, 90° ~ 120°, and the relative frequencies are 0.17 and 0.25, respectively. The crack directions of S4 are mostly distributed in 80° ~ 100° and 170° ~ 180°, and the relative frequencies are 0.21 and 0.13, respectively. The crack directions of S5 are mostly distributed in 80° ~ 100°, 170° ~ 180°, and the relative frequencies are 0.21 and 0.12, respectively. It can be concluded that the direction about initiation and propagation of cracks is relatively random. As for coral clay and Chongqing silt, cracks tend to develop horizontally and vertically, while cracks of talcum tend to develop horizontally.

Microscopic analysis

The macro-cracks divide the soil mass into clods of different shapes. We used an electron microscope to study the clods and found that there are still many microcracks in these soil clods. Different soils have different microcrack forms. In order to explore the distribution of microcracks in the soil, typical clods with a layer thickness of 15 mm are selected for microscopic analysis, as shown in Fig. 20.

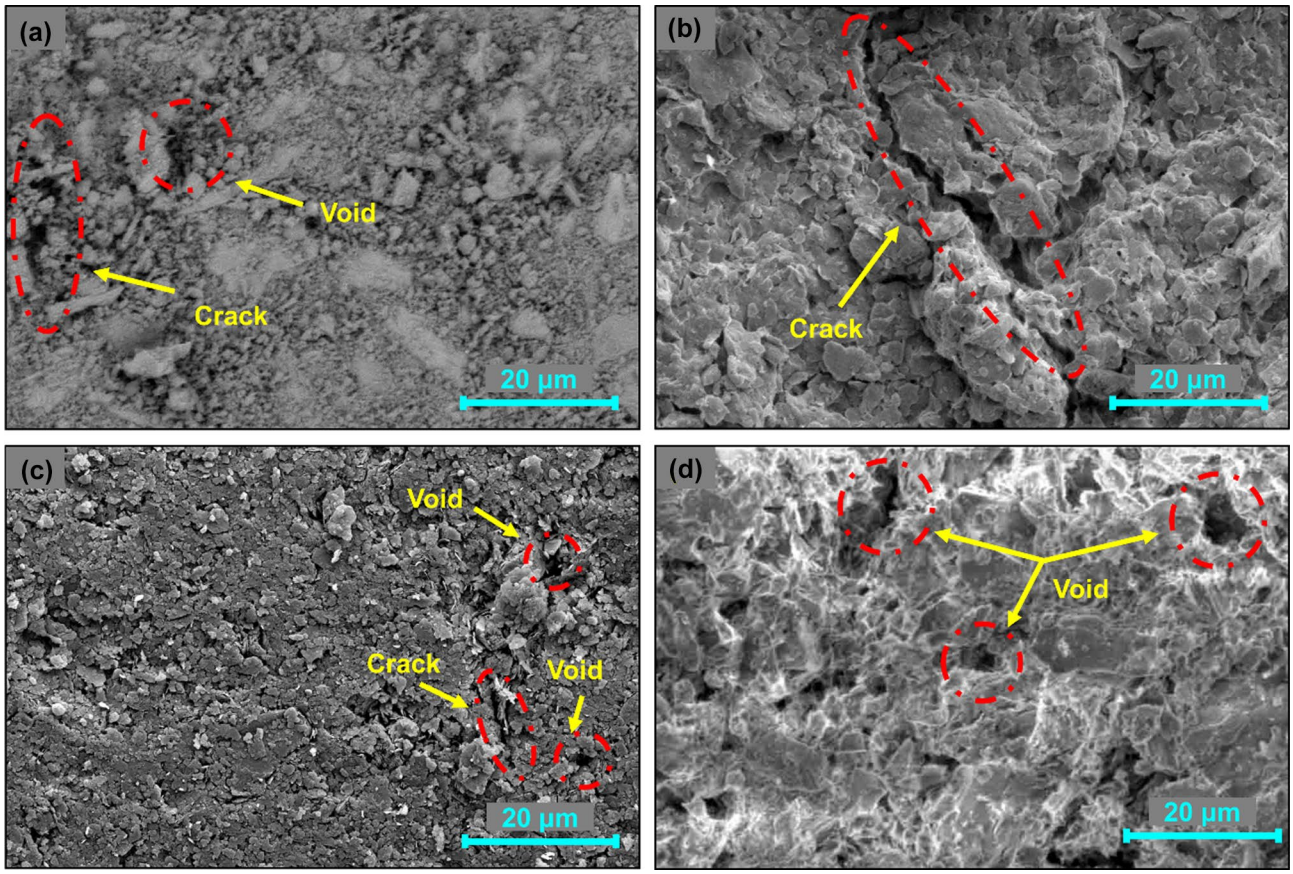

Fig. 20 The microscopic morphology of different soils with a layer thickness of 15 mm: **a** Coral clay; **b** Chongqing silt; **c** Kaolin; **d** Talcum

From Fig. 20(a), it can be seen that the surface distribution of coral clay is uneven, there are many pores, and also a few microcracks. It can be seen from Fig. 20(b) that Chongqing silt has microcracks that are longer than other soils under the same magnification. Due to the small area of the observed clod, it cannot be explained whether other soils also exist larger-scale microcracks. It can be observed from Fig. 20(c) that the surface of kaolin is more uniform and flatter than other soil surfaces, but there are also a small amount of micropores and microcracks. It can be seen from Fig. 20(d) that there are many micropores on the surface of talcum, which is due to the micropores

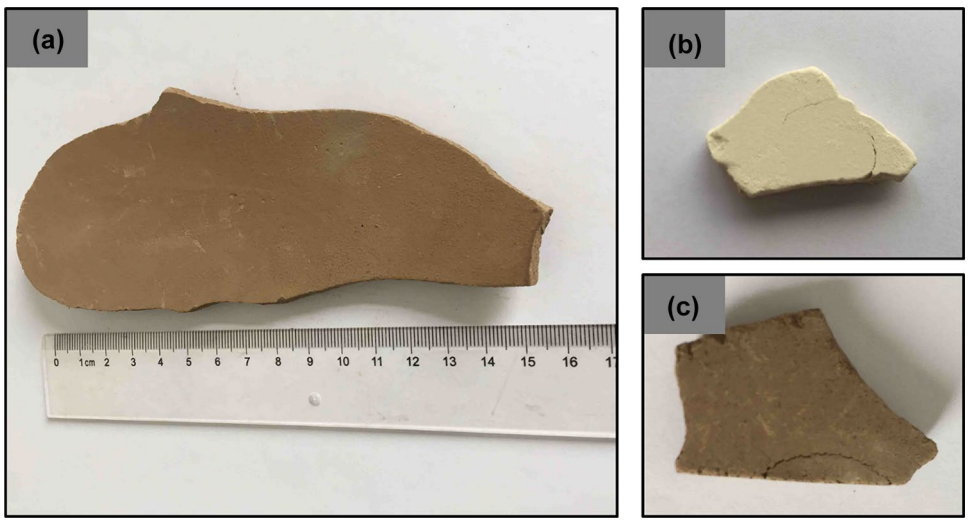

Fig. 21 Typical soil clods: **a** Soil clod warping; **b** and **c** Surface microcracks

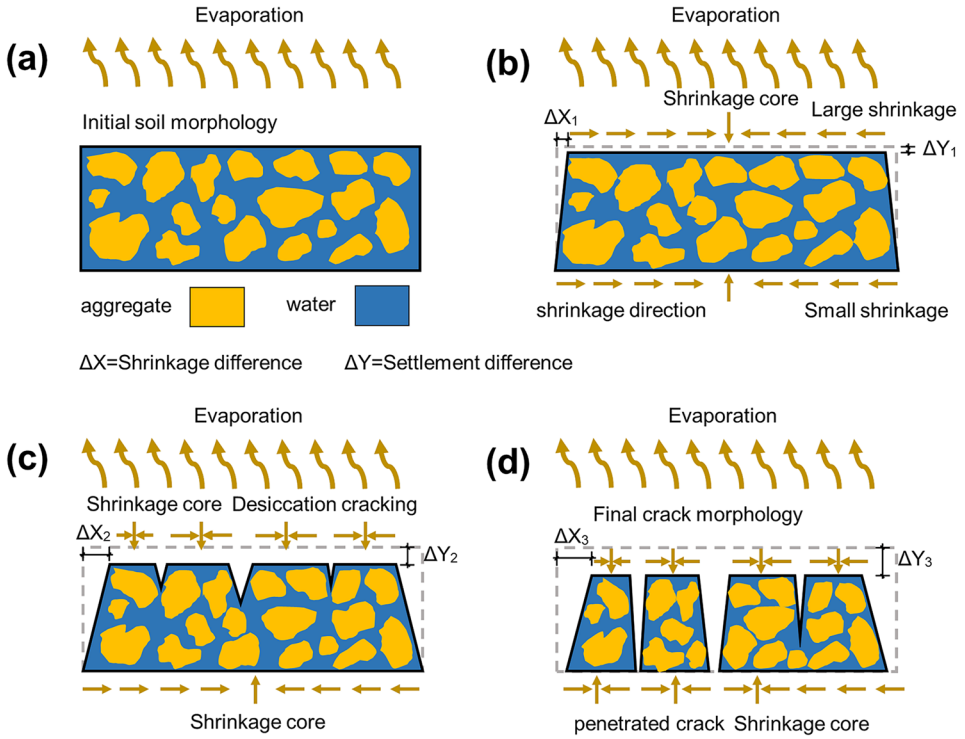

Fig. 22 Evolution mechanism of soil desiccation cracking

remaining when the gas escapes during the evaporation process, and then the microcracks start to initiate and propagate in the micropores. At present, the research on soil cracks mostly focuses on the quantitative analysis of macroscopic cracks, often ignoring the microcracks formed in the soil. The crack is the behavior when the surface tensile stress reaches the self-organized critical state, and the shape of the crack is often multi-scale.

Discussion on cracking mechanism

The initiation and propagation process of soil cracks is very complicated, which is significantly affected by the type and composition of the soil, layer thickness, and temperature (Tran et al. 2021; Tang et al. 2010).

It can be seen from Fig. 9 that kaolin has better anti-cracking performance compared with coral clay, Chongqing silt and talcum, and only small cracks are generated where bubbles escape and are perpendicular to the container wall. Coral clay, Chongqing silt and talcum contain different mineral compositions due to different soil types, so the resulting cracks vary greatly. The layer thickness also has obvious effects on the cracks of various soils. It can be observed that when the layer thickness of Chongqing silt is 15 mm, the edges of the large soil clod separated by the cracks have relatively obvious warping (Fig. 21(a)). This phenomenon also occur in other soils (Meng et al. 2020; Sánchez et al. 2019; Tran et al. 2019b). The clods of coral clay and Chongqing silt are separated by cracks that still have meso-cracks (Fig. 21(b), (c)). At the same time, we can still see microcracks (Fig. 20) by using a microscope. It can be seen that the type and composition of soil and the layer thickness have a significant impact on soil cracks, and the form of cracks is multi-scale, including macro-cracks, meso-cracks and microcracks. Therefore, it is necessary to discuss the cracking mechanism of soil.

Regarding the formation mechanism of soil cracks, there are viewpoints such as evaporation cracking, shrinkage

Table 1 Basic physical properties of different soils

Soil sample	Specific gravity	Liquid limit(%)	Plastic limit(%)	Plasticity index	Particle size analysis(%)		
					Sand	Silt	Clay
C	2.79	32.98	21.73	11.25	2	56	42
S	2.60	55.22	24.94	30.28	9	67	24
K	2.39	70.07	35.59	34.47	0	54	46
T	2.70	30.43	20.07	10.36	6	80	14

Table 2 Particle gradation parameters of different soils

Soil sample	d_{10}	d_{30}	d_{60}	C_u	C_c
C	0.001	0.003	0.011	11.000	0.818
S	0.003	0.006	0.017	5.667	0.706
K	0.002	0.004	0.007	3.500	1.143
T	0.004	0.011	0.028	7.000	1.080

Table 4 Types and contents of minerals in different soils

Soil sample	Types and contents of minerals(%)			
C	Aragonite	Calcite	Calcite magnesian	
	39.5%	35.5%	25%	
S	Quartz	Alurgite 2M1	Clinochlore 2 M	Albite, Ca-rich, ordered
	12.2%	19.3%	61.9%	6.6%

cracking, and air–water interface intrusion. For the non-cohesive fine-grained soil, (Shin and Santamarina 2011) believe that, driven by the increase of suction, the dry cracks in the fine-grained soil are generated as the air–water interface penetrates into the saturated medium. Subsequently, the interface film increases the local porosity ratio at the tip and decreases the air intake value. The air–water interface enters the tip, and the cracks grow. For cohesive soil, Tang et al. 2012 suggested that cracking is the result of mechanical action, essentially, which is a manifestation of soil tension failure. In the process of soil evaporation, it is often accompanied by shrinkage and cracking of the soil. Figure 22 is an evolution mechanism of soil desiccation cracking. The evaporation process will cause the migration and reduction of water in the soil. The state of soil will change from a saturated state to an unsaturated state. At the same time, due to the loss of water, the soil shrinks \Delta*x*, and settlement \Delta*y* will occurs on the surface of the soil sample. Due to the different type of soil, the shrinkage varies greatly. Kaolin has gone through the initial stage (Fig. 22 (a)), the surface settlement and shrinkage stage (Fig. 22(b)), and the surface microcrack development stage (Fig. 22(c)). In addition, the cracking phenomenon of kaolin is not obvious. Kaolin is extremely pure and has a small particle size, which results in a high viscosity. In the process of evaporative water loss, due to the good bonding between kaolin and the bottom and sides of the container, the soil shrinkage is greatly constrained by the bottom and sides of the container, which is the main reason for less propagation of cracks. Coral clay, Chongqing silt and talcum all have experienced the initial stage (Fig. 22(a)), surface settlement and contraction stage (Fig. 22(b)), crack initiation and propagation stage (Fig. 22(c)), and crack stable stage (Fig. 22(d)). Due to the different mineral compositions of these soils, there are differences in shrinkage, so the final cracks also show different morphological laws. In addition, temperature can accelerate the evaporation rate, which can promote the saturated soil to reach the plastic limit, shrinkage limit, etc. more quickly. As a result, cracks can be generated and developed earlier, and stabilized more quickly. The temperature has a significant effect on the final crack morphology, but the law is relatively insignificant. In the follow-up study, the mechanism needs to be further revealed.

As the moisture in the soil evaporates, the soil will transition from a saturated state to an unsaturated state. At this time, the matrix suction of the soil will gradually increase (Lu and Likos 2004). The unbalanced tensile stress field caused by matrix suction is the essential cause of the cracks. In the surface area where the soil particles are weakly connected, the tensile stress will be concentrated. Under the action of the concentrated tensile stress, the soil will move to the center of shrinkage. When the tensile stress in a certain part of the soil exceeds the connection strength or tensile strength of the soil, the connection among the particles will be broken, thereby forming a crack. The generation of cracks is also the release process of locally accumulated strain energy, so that the strain energy of the soil can be balanced again. After the cracks are generated, due to evaporation, the soil will shrink further. Furthermore, there is a stress concentration at the tip of the cracks, which will further expand the cracks and finally reach the stable stage of cracks. There are significant differences in the mineral composition,

Table 3 Types and contents of elements in different soils

Soil sample	Types and contents of elements (%)											
C	Ca	O	Mg	Sr	Na	Si	Fe	Sx	Cl	Al	K	Mo
	66.90	28.90	1.48	1.08	0.36	0.24	0.24	0.21	0.19	0.16	0.04	0.04
S	O	Si	Al	Fe	K	Mg	Ca	Na	Ti	S	P	Mn
	47.65	28.84	10.82	5	2.55	1.62	1.28	0.95	0.58	0.34	0.11	0.07
K	O	Si	Al	Ti	Fe	K	Mg	Na	Sx	Au	Pt	Mo
	50.17	25.19	23.44	0.37	0.30	0.17	0.12	0.07	0.05	0.03	0.03	0.02
T	Ca	O	Mg	Si	F	Sr	Al	Mo	Fe	Ru	Au	Rh
	53.82	32.91	6.36	6.30	0.36	0.05	0.05	0.04	0.02	0.02	0.01	0.01

Table 5 The main parameters of each soil sample

Soil sample	Temperature (℃)	Layer thickness(mm)
C1	30	5
C2	30	10
C3	30	15
C4	40	15
C5	50	15
S1	30	5
S2	30	10
S3	30	15
S4	40	15
S5	50	15
K1	30	5
K2	30	10
K3	30	15
T1	30	5
T2	30	10
T3	30	15

particle size, arrangement state, and mechanical properties (contact behavior, cementation, etc.) of soil particles about coral clay, Chongqing silt, kaolin and talcum. In addition, soils that appear homogeneous at the macroscopic level show great inhomogeneity at the microscopic level. These will significantly affect the cracking behavior of soils, resulting in significant differences in crack morphology.

Coral clay can be used as filler for foundations and slope protection projects, and can also be used for impermeable layers and wall layers. However, the desiccation cracking characteristics of coral clay will seriously deteriorate its engineering properties, resulting in deformation of the foundation, reduction in strength, instability of slope protection, failure of the anti-seepage function of the impermeable layer, and reduction of the protective function of the wall layer. So revealing the desiccation cracking mechanism is of great significance for the potential development value of coral clay. Our next work will be to improve the performance of coral clay, improve its mechanical properties and crack resistance, so as to promote the application of coral clay materials, improve the utilization rate of reef materials and realize their economic benefits.

Table 6 Fractal dimension

Soil sample	Fractal dimension	Linear regression coefficient
C1	1.628	0.9998
C2	1.690	0.9997
C3	1.749	0.9993
C4	1.759	0.9997
C5	1.786	0.9998
S1	1.612	0.9996
S2	1.824	0.9998
S3	1.901	0.9999
S4	1.902	0.9999
S5	1.920	0.9999
T1	1.778	0.9993
T2	1.784	0.9997
T3	1.824	0.9998

Conclusion

In this paper, a series of laboratory cracking tests were carried out to reveal the crack characteristics of coral clay, Chongqing silt, kaolin and talcum, with different layer thickness and temperature. The following conclusions were obtained:

1. Coral clay is a light yellow calcareous soft mud composed of fine-grained coral debris, belonging to low liquid limit clay. Its particle composition is mainly silt and clay, and its sand content is extremely low. Coral clay particles have a large size span, and there are a large number of flake clay particles, fine strip and needle-shaped particles distributed on the surface of large particles. Furthermore, the main chemical composition of coral clay is $CaCO_3$, and the main mineral components are Aragonite, Calcite and Calcite magnesian. The percentage of each mineral composition is 39.5%, 35.5%, and 25%, respectively.
2. The final shape of soils is significantly affected by the layer thickness and temperature. Coral clay, Chongqing silt and talcum with different layer thicknesses all showed significant crack networks. With the increase of layer thickness, the area of the soil clods divided by the cracks increases, while the number of soil clods decreases. However, the tiny cracks of kaolin have not propagated due to its large consistency.
3. The number of nodes of cracks decreases with the increment of the layer thickness. The law between the number of crack segments and the thickness of each layer thickness is more consistent with that of the number of nodes. The total length of cracks decreases with the increment of layer thickness. Coral clay shows a good linear law between the total length of cracks and the layer thickness. The average crack width of each soil increases with the increment of layer thickness, which shows a good linear relationship. Coral clay and Chongqing silt have relatively consistent changes in the number of clods and layer thickness. The total area of clods about coral clay slowly increases with the increase of layer thickness, while that of Chongqing silt shows the opposite pattern,

and that of talcum has little changed. The average area of clods about coral clay and Chongqing silt increases linearly and slowly with the increase of layer thickness. Coral clay, Chongqing silt and talcum show a linear increase in the maximum area of clods with the increase of layer thickness. The influence of temperature on the clod parameters and crack parameters of different soils varies greatly, and the law is relatively insignificant.

4. The fractal dimensions of coral clay, Chongqing silt and talcum all increase with the increment of layer thickness. Fractal dimensions of coral clay and Chongqing silt both increase slowly with the increase of temperature. Besides, the fractal dimension of coral clay and talcum has a good linear relationship with the layer thickness, while that of Chongqing silt shows a significant increase first and then slowly increase with the increment of the layer thickness. There is a good exponential relationship between the fractal dimension and the average crack width.
5. The layer thickness and temperature affect the morphological distribution of soil cracks. The frequency distribution of the crack length of coral clay and Chongqing silt and the frequency distribution of the crack width of coral clay all conform to the form of LogNormal function curve. The crack direction of initiation and propagation is relatively random. The cracks of coral clay and Chongqing silt tend to develop horizontally and vertically, while talcum cracks tend to develop horizontally. Moreover, the crack morphology is multi-scale, including macro-cracks, meso-cracks and microcracks.

Acknowledgements This work is supported by the National Natural Science Foundation of China (Grant Nos. 51878103 and 41831282), the Innovation Group Science Foundation of the Natural Science Foundation of Chongqing, China (Grant No. cstc2020jcyj-cxttX0003) and the Fundamental Research Funds for the Central Universities (Grant Nos. 2022CDJQY-012).

References

Abd El-Halim AA (2017) Image processing technique to assess the use of sugarcane pith to mitigate clayey soil cracks: Laboratory experiment. Soil till Res 169:138–145

An N, Tang CS, Cheng Q, Wang DY, Shi B (2020) Application of electrical resistivity method in the characterization of 2D desiccation cracking process of clayey soil. Eng Geol 265:105416

Baer JU, Kent TF, Anderson SH (2009) Image analysis and fractal geometry to characterize soil desiccation cracks. Geoderma 154:153–163

Bordoloi S, Hussain R, Gadi VK, Bora H, Sahoo L, Karangat R, Garg A, Sreedeep S (2018) Monitoring soil cracking and plant parameters for a mixed grass species. Geotech Lett 8:49–55

Bordoloi S, Ni J, Ng CWW (2020) Soil desiccation cracking and its characterization in vegetated soil: A perspective review. Sci Total Environ 729:138760

Cheng Q, Tang CS, Zeng H, Zhu C, An N, Shi B (2020) Effects of microstructure on desiccation cracking of a compacted soil. Eng Geol 265:105418

Colombi T, Kirchgessner N, Iseskog D, Alexandersson S, Larsbo M, Keller T (2021) A time-lapse imaging platform for quantification of soil crack development due to simulated root water uptake. Soil till Res 205:104769

Costa S, Kodikara J, Shannon B (2013) Salient factors controlling desiccation cracking of clay in laboratory experiments. Geotechnique 63:18–29

Emmanuel E, Anggraini V (2020) Effects of desiccation-induced cracking and leachate infiltration on the hydraulic conductivity of natural and olivine-treated marine clay. Int J Environ Sci Technol 17:2259–2278

Fang HQ, Jiang CY, Wang CL, Ou Q, Long KQ (2021) Effects of layer thickness and temperature on the crack morphology of Chongqing silt(in Chinese). Chin J Rock Mech Eng 40(12):2570–2583

Julina M, Thyagaraj T (2020) Combined effects of wet-dry cycles and interacting fluid on desiccation cracks and hydraulic conductivity of compacted clay. Eng Geol 267:105505

Knappett JA , Craig RF (2012) Craig's Soil Mechanics: 8th Edition.

Li JH, Zhang LM (2011) Study of desiccation crack initiation and development at ground surface. Eng Geol 123:347–358

Liu B, Zhu C, Tang CS, Xie YH, Yin LY, Cheng Q, Shi B (2020) Bioremediation of desiccation cracking in clayey soils through microbially induced calcite precipitation (MICP). Eng Geol 264:105389

Liu C, Tang CS, Shi B, Suo WB (2013) Automatic quantification of crack patterns by image processing. Comput Geosci 57:77–80

Lozada C, Caicedo B, Thorel L (2015) Effects of cracks and desiccation on the bearing capacity of soil deposits. Geotech Lett 5:112–117

Lu N, Likos WJ (2004) Unsaturated soil mechanics. Wiley

Luo ZG, Wang SJ, Yang ZB (2020) Quantitative analysis on fracture evolution of expansive soils under wetting-drying cycles effect(in Chinese). Rock and Soil Mechanics 41(07):2313–2323

Mei GX, Kumar H, Huang H, Cai WL, Reddy NG, Chen P, Garg A, Ganeshan SP (2020) Desiccation Cracks Mitigation Using Biomass Derived Carbon Produced from Aquatic Species in South China Sea. Waste Biomass Valor 12:1493–1505

Meng W, Liu M, Gan Y, Pauchard L, Chen C (2020) Cracking to curling transition in drying colloidal films. The European Physical Journal E 43:64

Mohammad N, Meng W, Zhang Y, Liu M, El-Zein A, Gan Y (2020) Desiccation Crack Formation and Prevention in Thin Bentonite Layers. Environ Geotech 1–14.

Niu YJ, Zhu HM, Yang SW, Ma SJ, Zhou JW, Chu B, Hua R, Hua LM (2019) Overgrazing leads to soil cracking that later triggers the severe degradation of alpine meadows on the Tibetan Plateau. Land Degrad Dev 30:1243–1257

Obada DO, Dodoo-Arhin D, Dauda M, Anafi FO, Ahmed AS, Ajayi OA, Csaki S, Bansod ND, Kirim II, Momoh OJ (2020) Crack behaviour and mechanical properties of thermally treated kaolin based ceramics: The influence of pore generating agents. Appl Clay Sci 194:105698

Pancrazi I, Ahmed H, Cerrano C, Montefalcone M (2020) Synergic effect of global thermal anomalies and local dredging activities on coral reefs of the Maldives. Mar Pollut Bull 160:111585

Peng Y, Ding XM, Xiao Y, Deng X, Deng WT (2019) Detailed amount of particle breakage in nonuniformly graded sands under one-dimensional compression. Can Geotech J 57:1239–1246

Peng Y, Liu HL, Li C, Ding XM, Deng X, Wang CY (2021) The detailed particle breakage around the pile in coral sand. Acta Geotech 16:1971–1981

Peron H, Laloui L, Hueckel T, Hu LB (2009) Desiccation cracking of soils. Eur J Environ Civ En 13:869–888

Qin ZG, Yuan XM, Cao ZZ, Mo HY (2021) Applicability and quality evaluation of foundation treatment method for backfilled coral sand site(in chinese). J Nat Disaster 30(01):78–88

Sánchez M, Al-Taie A (2020) Using Image Analysis Technique to Study the Effect of Boundary and Environment Conditions on Soil Cracking Mechanism. Geotech Geol Eng 39(1):25–36

Sánchez M, Al-Taie A, Zielinski M (2019) Experimental studies on curling development of artificial soils. J Rock Mech Geotech 11:1264–1273

Senior RB (1981) Tensile Strength, Tension Cracks, and Stability of Slopes. Soils Found 21:1–17

Shen Y, Feng ZY, Liu HL, Wang QC, An L (2018) Experimental study on effects of initial concentration on settling velocity characteristics of turbid surface of South China Sea coral mud(in chinese). Chinese Journal of Geotechnical Engineering 40:22–26

Shepidchenko T, Zhang JC, Tang X, Liu T, Dong Z, Zheng G, Yang L (2020) Experimental study of the main controlling factors of desiccation crack formation from mud to shale. J Petrol Sci Eng 194:107414

Shin H, Santamarina JC (2011) Desiccation cracks in saturated fine-grained soils: particle-level phenomena and effective-stress analysis. Geotechnique 61:961–972

Tang CS, Cheng Q, Leng T, Shi B, Zeng H, Inyang HI (2020) Effects of wetting-drying cycles and desiccation cracks on mechanical behavior of an unsaturated soil. Catena (giessen) 194:104721

Tang CS, Cui YJ, Tang AM, Shi B (2010) Experiment evidence on the temperature dependence of desiccation cracking behavior of clayey soils. Eng Geol 114(3):261–266

Tang CS, Shi B, Liu C (2012) Study on Desiccation Cracking Behaviour of Expansive Soil(in Chinese). J Eng Geol 20:663–673

Chen XS, Ding XM, Jiang CY, Fang HQ, Wang CL (2021) Experimental study on permeability characteristics of hydraulic reclamation calcareous clay in coral reef island(in chinese). Journal of Civil and Environmental Engineering 43(04):58–66

Tang CS, Zhu C, Leng T, Shi B, Cheng Q, Zen H (2019) Three-dimensional characterization of desiccation cracking behavior of compacted clayey soil using X-ray computed tomography. Eng Geol 255:1–10

Tran DK, Ralaizafisoloarivony N, Charlier R, Mercatoris B, Léonard A, Toye D, Degré A (2019a) Studying the effect of desiccation cracking on the evaporation process of a Luvisol – From a small-scale experimental and numerical approach. Soil till Res 193:142–152

Tran KM, Bui HH, Kodikara J, Sanchez M (2019b) Soil curling process and its influencing factors. Can Geotech J 57(3):408–422

Tran KM, Bui HH, Nguyen GD (2021) Hybrid discrete-continuum approach to model hydromechanical behavior of soil during desiccation. J Geotech Geoenviron Eng 147(10):04021102

Van Impe PO, Van Impe WF, Manzotti A, Mengé P, Van den Broeck M, Vinck K (2015) Compaction control and related stress–strain behaviour of off-shore land reclamations with calcareous sands. Soils Found 55:1474–1486

Wang C, Zhang ZY, Fan SM, Mwiya R, Xie MX (2018a) Effects of straw incorporation on desiccation cracking patterns and horizontal flow in cracked clay loam. Soil till Res 182:130–143

Wang LL, Tang CS, Shi B, Cui YJ, Zhang GQ, Hilary I (2018b) Nucleation and propagation mechanisms of soil desiccation cracks. Eng Geol 238:27–35

Wei X, Gao CY, Liu K (2020) A review of cracking behavior and mechanism in clayey soils related to desiccation. Adv Civ Eng 2020:1–12

Xie YK, Costa S, Zhou LM, Kandra H (2020) Mitigation of desiccation cracks in clay using fibre and enzyme. Bull Eng Geol Environ 79(8):4429–4440

Yin YP, Wang LQ, Zhang WG, Dai ZW (2022) Research on the collapse process of a thick-layer dangerous rock on the reservoir bank. Bull Eng Geol Environ 81(3).

Zainal K, Al-Madany I, Al-Sayed H, Khamis A, Al Shuhaby S, Al Hisaby A, Elhoussiny W, Khalaf E (2012) The cumulative impacts of reclamation and dredging on the marine ecology and land-use in the Kingdom of Bahrain. Mar Pollut Bull 64:1452–1458

Zeng H, Tang CS, Cheng Q, Inyang H, Rong DZ, Lin L, Shi B (2019) Coupling effects of interfacial friction and layer thickness on soil desiccation cracking behavior. Eng Geol 260:105220

Zeng H, Tang CS, Cheng Q, Zhu C, Yin LY, Shi B (2020) Drought-Induced Soil Desiccation Cracking Behavior With Consideration of Basal Friction and Layer Thickness. Water Resour Res 56:e2019WR026948.

Zhang J, Zhu D, Zhang SH (2020a) Shallow slope stability evolution during rainwater infiltration considering soil cracking state. Comput Geotech 117:103285

Zhang YP, Gu K, Li JW, Tang CS, Shen ZT, Shi B (2020b) Effect of biochar on desiccation cracking characteristics of clayey soils. Geoderma 364:114182

Zhang ZB, Peng X, Zhou H, Lin H, Sun H (2015) Characterizing preferential flow in cracked paddy soils using computed tomography and breakthrough curve. Soil till Res 146:53–65